Decadal variability in the Kuroshio-Oyashio Extension simulated in an eddy-resolving OGCM

Masami Nonaka,
Frontier Research Center for Global Change, JAMSTEC, Yokohama, JAPAN

Hisashi Nakamura,
Frontier Research Center for Global Change, JAMSTEC, Yokohama, JAPAN
also Graduate school of Science, the University of Tokyo, Tokyo, JAPAN

Youichi Tanimoto,
Frontier Research Center for Global Change, JAMSTEC, Yokohama, JAPAN
also Faculty of Environmental Earth Science, Hokkaido University, Sapporo, JAPAN

Takashi Kagimoto,
Frontier Research Center for Global Change, JAMSTEC, Yokohama, JAPAN

Hideharu Sasaki
The Earth Simulator Center, JAMSTEC, Yokohama, JAPAN

Submitted to *the Journal of Climate*

May 16, 2005
Revised on Aug. 17, 2005

Corresponding author address:
Masami Nonaka
Frontier Research Center for Global Change,
Japan Agency for Marine-Earth Science and Technology (JAMSTEC)
3173-25 Showa-machi, Kanazawa-ku, Yokohama, 236-0001 Japan
nona@jamstec.go.jp

ABSTRACT

Through analysis of a hindcast integration of an eddy-resolving quasi-global ocean general circulation model, decadal variability in the Kuroshio-Oyashio Extension region is investigated, with particular emphasis on that of the subarctic (Oyashio) and the Kuroshio Extension (KE) fronts. The KE front is deep and accompanied by sharp sea surface height (SSH) gradient with modest sea surface temperature (SST) gradient. In contrast, the subarctic front is shallow and recognized as a zone of tight gradient in SST but not SSH.

As a decadal-scale change from a warm period around 1970 to a cool period in the mid-1980s, those fronts in the model migrate southward as observed, and the associated pronounced cooling is confined mainly to those frontal zones. Reflecting the distinctive vertical structures of the fronts, the mixed-layer cooling is the strongest along the subarctic front, whereas the subsurface cooling and the associated salinity changes are the most pronounced along the KE front. Concomitantly with their southward migration, the two fronts have undergone decadal-scale intensification. Associated with reduced heat release into the atmosphere, the cooling in the frontal zones can be attributed neither to the direct atmospheric thermal forcing nor to the advective effect of the intensified KE current, while the advective effect by the intense Oyashio can contribute to the cooling in the subarctic frontal zone.

In fact, their time evolution is not found completely coherent, suggesting that their variability may be governed by different mechanisms. Decadal SSH variability in the KE frontal zone seems to be largely explained by propagation of baroclinic Rossby waves forced by anomalous Ekman pumping in the central North Pacific. This process alone cannot fully explain the corresponding variability in the subarctic frontal zone, where eastward propagating SSH anomalies off the Japanese coast seem to be superimposed on the Rossby wave signals.

1. Introduction

Since the pioneering works by Nitta and Yamada (1989) and Trenberth (1990), it has been established that the North Pacific (e.g., Tanimoto et al. 1993; Graham 1994; Kawamura 1994; Trenberth and Hurrell 1994) and the pan-Pacific (e.g., Zhang et al. 1997; Mantua et al. 1997) atmosphere-ocean coupled systems fluctuate on decadal and interdecadal time scales. One of the most prominent phase changes of the decadal variability over the Pacific Ocean occurred around 1977, which is called as a “climate shift” by some researchers. In association with the change, the tropical Pacific and the eastern North Pacific was warmed (e.g., Graham 1994), while sea surface temperature (SST) in the central North Pacific dropped significantly in association with intensified Aleutian low and surface westerlies.

Recent studies have revealed that the western North Pacific, more specifically, the so-called Kuroshio-Oyashio Extension (KOE) region is one of the primary centers of action of the decadal SST variability (Nakamura et al. 1997; Schneider et al. 2002; Schneider and Cornuelle 2005). From a macroscopic view the KOE region is a zonally oriented SST frontal zone associated with strong eastward surface currents, forming the boundary of the oceanic subtropical and the subpolar gyres (e.g., Yasuda et al. 1996). Detailed investigations have shown that SST anomalies (SSTAs) in the KOE region (more specifically, the subarctic frontal zone) associated with decadal variability exhibit no significant simultaneous correlation with those either in the subtropical central North Pacific (specifically, in the subtropical frontal zone) or in the tropical Pacific (Nakamura et al. 1997; Nakamura and Yamagata 1999; Tomita et al. 2001). Rather, SSTAs in the subarctic frontal zone tends to lag by about five years to those in the subtropical frontal zone (Miller and Schneider 2000).

It has also been argued that air-sea interaction in the KOE region has the potential to force (Latif and Barnett, 1994) or intensify (Barnett et al. 1999; Pierce et al. 2001; Schneider et al. 2002) the decadal variability in the North Pacific. Concerning the atmospheric responses to the

midlatitude SSTAs that are necessary for the interaction, however, atmospheric general circulation model studies have still failed to show coherent responses and most of observed data analyzing studies have shown dominance of atmospheric forcing to SSTAs in most of the extratropics (Kushnir et al. 2002, for recent review). Nevertheless, recent analyses of observed data have suggested the existence of the ocean-to-atmosphere feedback in the KOE region (Nonaka and Xie 2003; Tanimoto et al. 2003).

In addition to the atmospheric response, how decadal-scale SSTAs are induced in the KOE region also needs to be clarified. It is well known that wintertime SSTAs are primarily forced by the atmospheric variability through surface heat flux anomalies in most of the central and eastern North Pacific (e.g., Cayan 1992; Alexander 1992). However, it has recently been shown by oceanic general circulation model (OGCM) studies (Xie et al. 2000; Yasuda and Kitamura 2003) and suggested by observational studies (Qiu 2000; Tomita et al. 2002; Kelly and Dong 2004) that SSTAs in the KOE region can be generated through oceanic dynamics.

Three mechanisms have been proposed on the generation of decadal-scale SSTAs in the KOE region. First, Latif and Barnett (1994) proposed that anomalous warm-water transport from the tropics by the Kuroshio and its extension current associated with spin-up/spin-down of the subtropical gyre induces SSTAs in the KOE region. This mechanism is consistent with an analysis by Qiu (2000) of the heat budget in the Kuroshio Extension (KE) region based on observational data. Second, propagation of oceanic Rossby waves forced by anomalous wind stress curl (and associated Ekman pumping) can induce perturbations in the thermocline depth within the KOE region (Masuda 2003), producing SSTAs there (Schneider and Miller 2001). Third, Seager et al. (2001) suggested through their analyses of an OGCM output and observed data that meridional migration of the KOE SST front can be caused by propagation of wind induced Rossby waves that have been forced by Ekman pumping anomalies around the boundary between the gyres. The last two hypotheses can explain the five-year lag observed between

decadal-scale SSTAs in the central North Pacific and the KOE region as the traveling time of the Rossby waves (Seager et al. 2001; Schneider et al. 2002).

In the previous studies mentioned above, the analyzed data that are based on a paucity of observations or OGCM integrations under limited computational resources have rather coarse horizontal resolutions for basin-scale temperature changes. The resolutions of those data, however, are not high enough to resolve the complex structure of the KOE frontal zone, as suggested by satellite data (Nakamura and Kazmin 2003). In fact, detailed analyses of observed temperature fields have revealed that there are at least two prominent fronts in the KOE region: the KE front along the KE current (e.g., Mizuno and White 1983) and the subarctic (Oyashio) front associated with the Oyashio Extension current (e.g., Yuan and Tally 1996). Those two fronts are meridionally separated by the Kuroshio-Oyashio mixed water region (Yasuda et al. 1996, and references therein). Variability of the two fronts could be governed by different dynamics, and if so, they would not necessarily vary in a coherent manner as simulated in the GCM experiments with coarse horizontal resolutions in the previous studies.

In this study, we investigate how each of the fronts in the KOE region changes in association with decadal basin-scale variability in the North Pacific and how well the mechanisms currently proposed for the North Pacific decadal variability can be applied to the KOE region. Our analysis is based on a hindcast OGCM experiment performed on the Earth Simulator (Ohfuchi et al. 2005), whose high computational performance allows us to integrate the model over 54 years with such a high resolution as to resolve the separation of those two fronts adequately. Our analyses indicate that the strongest decadal-scale temperature anomalies simulated in the surface (subsurface) layer are generated in association with decadal changes in the subarctic (KE) fronts, indicating the primary importance of oceanic processes in inducing the thermal anomalies there.

The paper is organized as follows. Section 2 describes the model and datasets. Section 3 compares our OGCM fields with observations. Section 4 presents typical anomalies in the

temperature field and the fronts associated with the North Pacific decadal variability. Temporal developments of the decadal anomalies are also reported there. Section 5 discusses some mechanisms for the changes. Section 6 provides a summary.

2. Model and datasets

a. *The OFES*

The OGCM we use in this study is the Modular Ocean Model (MOM3) (Pacanowski and Griffies, 2000), developed at the Geophysical Fluid Dynamics Laboratory/National Ocean and Atmospheric Administration (GFDL/NOAA). The code has been substantially modified for attaining its efficient performance on a vector-parallel hardware system of the Earth Simulator. Our ocean model for the Earth Simulator (OFES; Masumoto et al. 2004) covers a near-global domain extending from 75°S to 75°N, except for the Arctic Ocean, with horizontal resolution of 1/10°. The model has 54 vertical levels, with resolutions from 5 m at the surface to 330 m near the bottom. The model topography is based on the 1/30° bathymetry dataset (kindly provided by GFDL/NOAA) with the maximum depth of 6,065 m.

The model solves the primitive equation system in spherical coordinates under the Boussinesq and hydrostatic approximations. The KPP boundary layer mixing scheme (Large et al. 1994) is adopted for vertical mixing. For horizontal mixing of momentum and tracers, we adopt a scale-selective damping with a bi-harmonic operator, to suppress grid-scale computational noises (Smith et al. 2000). The background horizontal bi-harmonic viscosity and diffusivity are -27×10^9 $m^4 s^{-1}$ and -9×10^9 $m^4 s^{-1}$, respectively. These values are the same as those used in Maltrud and McClean (2005) and Smith et al. (2000) for 0.1°-resolution global and Atlantic OGCMs, respectively, but suitability of the values and sensitivity of the solution to the values need to be explored further in future studies.

In the model, the surface heat flux is calculated with the bulk formula by Rosati and

Miyakoda (1988) from atmospheric variables based on the National Centers for Environmental Prediction/National Center for Atmospheric Research (NCEP/NCAR) reanalysis (Kalnay et al. 1996). The fresh water flux is evaluated from daily precipitation rate taken from the reanalysis data, under the constraint for sea-surface salinity to be restored to its monthly climatology with time-scale of 6 days, to include the contribution from river run-off. The climatology is based on World Ocean Atlas 1998 (WOA98; Boyer et al. 1998a, 1998b, 1998c). Within 3° from the model's artificial boundaries placed at 75°N and 75°S, temperature and salinity are restored to their local monthly climatologies (WOA98) with time scale that is 1 day at the boundaries and increasing to infinity into the interior region. See Masumoto et al. (2004) and Sasaki et al. (2005, in preparation) for details of the model set up.

The model was integrated for 50 years from the climatological annual-mean fields of temperature and salinity (WOA98) without motion by applying the climatological monthly-mean atmospheric forcing for the period from 1950 to 1999 based on the NCEP/NCAR reanalysis data. Following this 50-year climatological run as the model spin-up, we conducted a 54-year hindcast integration with daily mean atmospheric fields of the NCEP/NCAR reanalysis data from 1950 to 2003. In the following analyses, model climatology and anomaly are defined as mean for this 54-year period and deviation from it, respectively.

Smith et al. (2000) showed that with 0.1° horizontal resolutions mesoscale eddies should be resolved reasonably well. For our analytical convenience, however, the full resolution (0.1°) of the model output has been reduced to 0.5° resolution by picking up the data at every five grid-points both in the zonal and meridional directions. Though reduced, the resolution is still adequate for resolving fine frontal structures in the KOE region as shown below, and variability in frontal structures in the SST and sea surface height (SSH) fields discussed below is confirmed to have the same characteristics between the reduced and full resolution datasets.

b. Observational datasets

In addition to the output of the hindcast integration of the OFES, we also use the following observed ocean temperature data products: the Japan Meteorological Agency (JMA) SST data set, Frontier Research System-Comprehensive Ocean and Atmosphere Data Set (FRS-COADS; Tanimoto and Xie 2002), White's (1995) temperature data set, and the World Ocean Atlas 2001 (WOA2001; Stephens et al. 2002). The JMA-SST data have been compiled for the western North Pacific (100°-180°E, 0°-60°N) with 1° horizontal resolutions by JMA based on subjective analysis of in-situ and satellite observations for every 10-day period from 1950 to 1999[1]. The FRS-COADS is a gridded dataset with 2°x2° resolution constructed for every 10-day period based on quality-controlled ship and buoy measurements that has been compiled in the Long Marine Reports in fixed length records (LMRF) of the Comprehensive Ocean-Atmosphere Dataset (COADS; Woodruff et al. 1987). We use monthly mean SST fields based on the FRS-COADS for the period from 1950 to 1995. White's dataset contains monthly-mean temperature fields both at the sea surface and subsurface levels (20, 40, 60, 80, 120, 160, 200, 240, 300, and 400 m deep) from 1955 to 2002 with the zonal and meridional resolutions of 5° and 2°, respectively, based on hydrographic observations. The WOA2001 contains the monthly climatologies of objectively analyzed temperature data on a 1°x1° latitude-longitude grid at the standard depth levels. We also use monthly-mean SST fields based on measurements by the Advanced Microwave Scanning Radiometer (AMSR-E) on the Aqua satellite. The dataset has been produced by the Remote Sensing Systems with horizontal resolutions of 0.25°.

[1] The JMA-SST data include satellite data since 1998, yielding a discontinuity in the data quality in that year. It has, however, little influence on our analyses because we focus primarily on earlier years in this study.

3. Observed and simulated decadal variability in the northwestern Pacific

a. *Fine frontal structures in the KOE region*

Figure 1 shows a mean SST field simulated in the OFES for a particular month and the corresponding field based on the AMSR-E measurements. This figure indicates that, with its eddy resolving resolutions, the OFES is successful in reproducing not only the separations of the Kuroshio and Oyashio Currents from the western boundary but also the meridional separation of two sharp SST fronts along with their extensions unambiguously. As in the observation (e.g., Mizuno and White 1983), the KE front in the model forms along the KE current meandering around 35°N as the eastward continuation of the Kuroshio Current off Japan. As observed, the subarctic front in the model forms around 42°N along the Oyashio Current and its extension. As revealed in satellite data (Nakamura and Kazmin 2003), these two fronts are separated by a region of relatively uniform SST into which warm and cold eddies are cut off. Although the subarctic front in the OFES appears to be too strong to the east of about 160°E compared to the AMSR-E observation, Yuan and Talley (1996, their Fig. 12) showed that SST gradient across the front often exceeds 5°C/100 km, suggesting that the simulated gradient may not necessarily unrealistic. The successful reproduction of the two fronts in the OFES gives us the first opportunity to investigate how each of the fronts varies on decadal time scales and their role in causing large-scale SSTAs in the KOE region.

b. *Surface and subsurface fronts*

Figure 2 shows meridional sections of wintertime (January-March) climatological temperature based on the OFES and WOA 2001. In the observed climatology (right panel), the KE and subarctic fronts are found around 35°N and to the north of 40°N, respectively. Though diffused perhaps due to the sparseness of subsurface observations, there are two maxima of meridional temperature gradient, one in the surface layer across the subarctic front and the other

between 300 and 400-m depths associated with the KE front. Obviously, the OFES (left panel) can also reproduce subsurface temperature distributions in the KOE region reasonably well, including the latitudinal positions and vertical distributions of the two fronts. In the OFES climatology, the meridional separation of the two fronts and their distinctive vertical structures are much more apparent. The KE front has a deep structure with its maximum meridional temperature gradient below the 300-m depth and relatively weak SST gradient, while the subarctic front is shallow with its maximum gradient just below the sea surface.

c. *Decadal-scale temperature variability in the KOE region*

In Fig. 3, five-year running mean time series of area-mean wintertime temperature in the KOE region, [35°-43°N, 140°-170°E] are compared between the observational datasets and the OFES simulation. The top panel indicates that the OFES simulation (solid curve) captures the characteristics of the observed decadal SST variability as represented in the FRS-COADS (long-dashed) and White's (dashed) datasets, including cool periods in the early 1960s and in the mid-1980s, and warm periods around 1970 and in the 1990s. At the same time, it is also apparent that the OFES SST has a slight cooling trend throughout the integration period.

The middle and bottom panels of Fig. 3 show the observed and simulated decadal variability in surface and subsurface temperature. As suggested by Deser et al. (1996) and by Schneider and Miller (2001), the decadal temperature variability in the KOE region was coherent between the surface and subsurface levels (bottom panel), and so it is in the OFES simulation (middle panel). The time series show that a pronounced cool period in the 1980s and a relatively warm period in the early 1970s are well represented in the OFES. While the profound warming in the late 1980s is well simulated in the OFES, the simulated temperature anomalies are negative in the 1990s, as opposed to the observation, in the presence of the cooling trend in the model. The decadal-scale cooling in the 1960s, which is apparent in the OFES simulation as in the FRS-COADS SST data,

is not particularly obvious in White's data, which may be due to the paucity of observations in the early period. In short, except for the unrealistic cooling trend, the OFES can reproduce the decadal temperature variability in the KOE region not only at the surface but also in the subsurface layers.

4. Decadal-scale changes in the fronts in relation to temperature anomalies in the KOE region

a. *Decadal SST anomalies*

In this section, the decadal variability in the North Pacific is examined in more detail, highlighting the differences between a pair of five-winter mean fields for the 1968-72 and 1984-88 periods. These two periods correspond to the well-defined warm and cool phases, respectively, associated with the decadal variability in the KOE region, as shown in Fig. 5 of Nakamura et al. (1997). Maps of the SST difference observed and simulated over the North Pacific between the two periods are plotted in Fig. 4, superimposed on the corresponding mean SST field for the latter period. In Fig. 4, the mean and anomaly fields of SST in the OFES simulation are compared with those for the FRS-COADS data. As in the snapshot shown in Fig. 1, the mean SST field (contours) is overall reproduced well in the OFES, while a number of meso-scale structures associated with eddies and current meanders are apparent in the OFES simulation, even in its five-winter mean field. These meso-scale eddies are smoothed out completely in the observed SST field due to its lower horizontal resolution.

Large-scale features of decadal-scale SST anomalies, as represented in SST differences between the two periods, are also well represented in the OFES simulation. Consistent with the previous observational studies (e.g., Tanimoto et al. 1993; Nakamura et al. 1997), well-defined cool anomalies are distributed in the western and central portions of the North Pacific with their zonally extended cold core around 40°N, whereas warm anomalies are confined to the eastern

North Pacific off the west coast of North America. Since we chose the particular periods with the strongest SST anomalies in the KOE region (Nakamura et al. 1997), the cool anomalies in the central North Pacific are relatively weak compared to a typical SSTA pattern associated with the Pacific Decadal Oscillation (Mantua et al. 1997).

In the OFES SST field, the KE and subarctic fronts are clearly separated from one another even in the five-winter mean, and the decadal anomalies in the KOE region are the strongest along the fronts. A close comparison reveals that SST gradient is stronger across the subarctic front than across the KE front, and so are the associated SST anomalies, as indicated in satellite data by Nakamura and Kazmin (2003). There are, however, some unrealistic features in the simulated SSTAs, for example, off the Chinese coast and south of Japan. The discrepancy to the south of Japan is due to Kuroshio meanders, which are not directly controlled by large-scale winds and are unrealistically simulated in the OFES.

b. *Decadal changes in the surface fronts*

The confinement of strong SSTAs to the surface frontal zones as shown in Fig. 4 suggests that the anomalies may be associated with decadal shifts in the frontal positions. Figure 5 shows magnitudes of the horizontal SST gradient for the two five-year periods of our interest based on the OFES simulation. In each of the periods, the SST gradient is the strongest along the subarctic front around 40°N, and it is much weaker along the KE front located to its south. In the bottom panel of Fig. 5, SST gradient fields for the earlier (1968-72; contoured) and later (1984-88; shaded) periods are superimposed to illustrate decadal changes in the frontal positions. It is apparent in that panel that those two fronts both migrate southward, while somewhat intensified from the earlier to the later period. In agreement with an analysis of satellite data by Nakamura and Kazmin (2003), the subarctic front has been shifted southward 2~3° in latitude while keeping its southwest-to-northeast orientation. Meanwhile, the southwest-to-northeast orientation of the

KE front apparent in the earlier period has been changed into the more zonal orientation in the later period. This particular change is manifested as the increasing southward shift of the frontal axis with longitude. The shift reaches as much as 5° in latitude around 165°E, suggestive of decadal changes in the KE current. The southward migration of the frontal axes mentioned above strongly suggests that the migration has induced the strong cooling tendency from the 1970s to the 1980s simulated along the fronts. Additionally, the frontal migration yields stronger SSTAs around the subarctic front than around the KE front, reflecting stronger frontal intensity of the former.

To examine whether the aforementioned changes in the fronts are limited to the surface temperature field, we further look into changes in the horizontal gradient of SSH in Fig. 6 between the two periods as in Fig. 5. As opposed to the SST field in Fig. 5, the horizontal SSH gradient is much stronger across the KE front than across the subarctic front. Nevertheless, the southward migration of the two SST fronts found in Fig. 5 is also recognized in Fig. 6, indicating that the frontal changes are not limited to the surface thermal field but rather associated with changes in the gyre circulation. As in the SST field (Fig. 5), the magnitude of the SSH gradient is slightly intensified to the west of 170°E across the subarctic front (Fig. 6). Across the KE front, by contrast, the SSH gradient has been strongly intensified to the east of 150°E, in addition to the southward migration of the frontal axis and changes in its orientation as found in the SST field. The difference found in the decadal changes between the two fronts in the KOE region suggests that their changes could arise from different mechanisms.

In association with the SSH gradient changes, the surface velocity fields has also changed between the two periods (Fig. 7). Consistent with the enhanced SSH gradient of the KE front and the change of its axis into more zonal orientation into the later period, the KE current has been intensified especially between 150°E and 170°E, and it flows eastward around 35°N in the later period. Though not so significant as the KE current, an eastward current along the subarctic front

(Oyashio Extension) is also stronger in the later period between 150°E and 170°E. Furthermore, a southwestward Oyashio current along the Kuril Islands has also intensified slightly into the later period.

c. *Changes in subsurface frontal structures*

The aforementioned decadal-scale changes in the SSH fronts may be associated with some changes in dynamical fields that are likely to accompany the corresponding changes in subsurface thermal fields. In Fig. 8, we plot meridional sections of five-winter mean temperature (left) and salinity (right) simulated for the three periods, 1968-72, 1976-80 and 1984-88, with the corresponding anomaly fields as deviations from their 1950-2003 climatological mean fields. In each of the periods, the two fronts located at ~35°N and ~43°N exhibit their distinctive vertical structures in the subsurface temperature field, as found in the climatological mean field (Fig. 2). Comparing the top and bottom panels in the left column of Fig. 8, one can recognize southward migration of the subarctic and KE fronts into the later period also at subsurface levels, in a manner consistent with what is indicated in the SST and SSH gradient field. In association with their migration, pronounced temperature anomalies form below the surface along their axes in those two periods. The anomalies associated with the subarctic front are the strongest near the surface, while the strongest anomalies associated with the KE front are located 300~500 m below the surface. This difference reflects the corresponding difference in the vertical structure of the two fronts as mentioned in section 3.

Interestingly, in the OFES simulation, decadal-scale cool anomalies first emerge within the near-surface subpolar gyre in the late 1970s (middle-left panel of Fig. 8) before the strongest cooling occurring in the early 1980s along the two fronts. In the late 1970s, warm anomalies still remain along the entire depth of the KE front, and the preceded cool anomalies in the subpolar gyre seem to accompany no substantial salinity anomalies (middle-right panel). Nakamura et al.

(1997) pointed out that surface cooling in the subarctic frontal zone started as early as 1974, based on the COADS data.

The corresponding meridional sections of salinity for those periods (right panels of Fig. 8) indicate that the subarctic and KE fronts can also be recognized as salinity fronts. The southward migration of the fronts from the earlier to the later period yields vertically coherent salinity anomalies around the frontal axes. As the corresponding thermal anomalies, those salinity anomalies in the subarctic frontal zone are the strongest in the surface layer and decaying downward, while the strongest anomalies are located 300~400 m below the surface in the KE frontal zone. These frontal changes in the salinity fields also suggest that the temperature changes may be induced not only by direct atmospheric thermal forcing but rather by the frontal changes.

d. *Changes in frontal intensity*

Meridional sections of simulated temperature (contours) and its meridional gradient (colored) zonally averaged between 145°E and 160°E (Fig. 9, left panels) clearly show the intensification of the KE front and its aforementioned southward migration from the earlier period (1968-72) into the later period (1984-88). In association with these changes, the thermocline located between the two fronts has moved upward, and the region to the north of the KE front has cooled into the later period (color contours in the lower-left panel), while the south of the front has slightly warmed.

The intensification of the KE front in the later period is associated with the enhanced KE current (Fig. 7) that can transport warm temperature water more than in the earlier period. The collocation of the cool anomalies and the enhanced warm current in the large part of the KOE region clearly denies the notion that the enhancement of the warm advection is the cause of the temperature anomalies in the 1980s. This notion, however, may be applicable to the 1990s, in which warm anomalies to the south of the intensified KE front are in conjunction with the

intensified KE current and the associated deepening of the thermocline to the south.

The corresponding meridional sections are given in the right panels of Fig. 9, based on White's observed temperature dataset. Owing to its coarser resolution, the fronts are apparently diffused compared to those in the OFES simulation and so are the changes in the strength of the KE front. Nevertheless, one can recognize the enhancement of the meridional temperature gradient across the KE front in the later period (1984-88), which is consistent with the intensified KE current in the later period, as pointed out in the previous studies based on analyses of observed fields of subsurface temperature (Miller et al. 1998) and wind (Deser et al. 1999). Concomitantly, the cooling was observed mainly to the north of the KE front, which is particularly apparent in the surface (subsurface) layer in the subarctic (KE) front region. While the southward migration of the subarctic front in the cool period is evident in White's data, no such migration is apparent for the KE front in the same data whose 2° meridional resolution may be too coarse. In fact, the southward migration of a frontal zone in the KOE region is noticeable in the JMA-SST data with 1° resolution (Nakamura and Kazmin 2003).

The results shown in this subsection suggest that both the gyre boundary migration (Seager et al. 2001) and vertical thermocline displacement (e.g., Schneider and Miller 2001) mechanisms seem to be operative in inducing the decadal cooling simulated in the KOE region from the 1970s to the mid-1980s, whereas changes in warm water advection are unlikely so, as suggested from the observed data.

e. Seasonal dependence

Thus far we have focused on wintertime features of the decadal-scale thermal anomalies in the KOE region. In this subsection, we examine the seasonality of those anomalies by comparing between their wintertime and summertime composites.

Figure 10 depicts summertime (July-September) distribution of SST averaged over the

1984-88 period (contoured) and its difference (shading) from its counterpart for another five-year period of 1968-72, based on the observed data (top panel) and the OFES simulation (bottom panel). In agreement with previous observational studies (e.g., Norris et al. 1998; Nakamura and Yamagata 1999), the figure indicates that both the observed and simulated decadal-scale SSTAs, as extracted in the difference maps, are zonally elongated almost across the midlatitude Pacific basin in a manner more or less similar to that in their wintertime counterpart (Fig. 4). The observed summertime decadal SSTAs are overall reproduced well in the model with respect to their spatial distribution and amplitude (Fig. 10). In contrast to their wintertime counterpart (Fig. 4), the simulated summertime SSTAs and their confinement to the SST fronts are substantially weaker (Fig. 10). In summer, surface heat flux is downward over the North Pacific to render the mixed layer much shallower than in winter. For the heat budget in the shallow mixed layer, contributions from ocean currents and ocean dynamics are less important compared to the contribution of the surface heat flux (e.g., Tomita et al. 2002). Therefore, SST gradient across the fronts and SSTAs in the frontal zones cannot be as strong as in winter. In fact, the AMSR-E measurements reveal that the SST gradient across the subarctic front is indeed weaker in summer than in winter (figures not shown). Though not as pronounced as in the OFES simulation, the observed SSTAs also exhibit summertime weakening along the subarctic frontal zone (top panels between Figs. 4 and 10), while summertime SST frontal intensity is almost the same as the counterpart in wintertime that is consistent with the finding of Nakamura and Kazmin (2003). Exploring the mechanism for the seasonal change in the subarctic front is still a subject of our future work.

We have shown that the decadal-scale cooling observed and simulated along the frontal zones in the KOE region is substantially weaker in summer than in winter. In the subsurface layers, however, that is not the case, at least in the model (Fig. 11). In the top panel of Fig. 11, wintertime (January-March) temperature simulated at 150-m depth is plotted with contours as an

average for the 1984-88 period, on which its difference from another period of 1968-72 is superimposed with colors. Comparing with the corresponding SSTAs (Fig. 4, bottom panel), the confinement of the decadal-scale thermal anomalies to the subarctic and KE fronts, as extracted in the difference map, is enhanced in the subsurface layer. In fact, no pronounced subsurface anomalies are found over the eastern half of the basin, where no major frontal zones are present. This is an indication that the wintertime decadal SSTAs over that region are generated directly by the atmospheric forcing. The corresponding summertime (July-September; lower panel of Fig. 11) subsurface temperature and its anomalies are almost identical to those in winter (upper panel) indicative of the remarkable persistency of the decadal-scale subsurface thermal anomalies along the two fronts. This is probably because those subsurface layers are isolated from summertime heating by a shallow seasonally developed thermocline. It should be stressed that the frontal confinement of decadal-scale thermal anomalies is also apparent in the layer below the bottom of the wintertime mixed layer (not shown). It is suggested that those temperature anomalies are induced by decadal-scale migration of the frontal axes and thus retained throughout summer below the seasonal thermocline.

Those subsurface anomalies would emerge into the mixed layer as it deepens in winter. While the re-emergence of temperature anomalies in the North Pacific associated with deep winter mixed layer (Alexander et al. 1999) and its role in the decadal variability has been pointed out (Deser et al. 2002; Newman et al. 2003), the present study suggests that the re-emergence of subsurface thermal anomalies can also occur due to decadal-scale migration of a frontal axis and associated thermocline changes in association with changes in the oceanic dynamical field, as proposed by Schneider and Miller (2001). It is noteworthy that in this particular mechanism, unlike in the Namias-Born (1974) mechanism, temperature anomalies can remain throughout the year even in the layer below the wintertime mixed layer bottom.

f. *Longitude-time sections*

To further examine the decadal variations in the KOE regions, we plot longitude-time sections of simulated SSH anomalies in Fig. 12 for 36°N and 43°N, which roughly correspond to the KE and subarctic fronts, respectively. As Nakamura and Kazmin (2003) found in the observed SST anomalies, the simulated SSH anomalies in the KOE region are dominated by decadal-scale variability rather than by interannual one. As discussed above, the positive and negative anomalies around 1970 and 1986, respectively, are evident at each of the latitudes. Those decadal-scale SSH anomalies tend to propagate westward faster at 36°N than at 43°N. Their propagation are more or less consistent with the theoretical propagation speeds of the first baroclinic long Rossby waves at the corresponding latitudes, as indicated with a heavy black straight line in Fig. 12. A close inspection of Fig. 12 reveals that propagation speeds in the simulation tend to be slightly higher than their theoretical counterpart, as actually observed (Chelton and Schlax 1996). A comparison between the anomalies in the central-to-eastern portion of the basin at the two latitudes reveals that the decadal-scale SSH anomalies tend to appear earlier at 43°N than at 36°N, while the time lag becomes short in the western basin because of the slower propagation at 43°N.

In addition to the prevailing westward propagating anomalies, there seem to be eastward propagating SSH signals from ~150°E to ~170°E in the section for 43°N (but not at 36°N). As indicated in the right panel of Fig. 12 with white lines, two positive events around 1970 and 1990 and a negative event of eastward propagation in the mid-1970s are noticeable. It is suggested with these signals in the OFES simulation that decadal-scale SSH anomalies in the subarctic frontal zone tend to emerge both in the eastern and western portions of the basin almost simultaneously and then propagate westward and eastward, respectively, until they merge together around 170°E, where the anomalies tend to be the strongest. The presence of such

eastward propagating signals along the subarctic frontal zone as in the OFES simulation is suggested in the JMA-SST data. A lag correlation map of decadal-scale SST fluctuations with the time index of the first empirical orthogonal function (EOF) of the western North Pacific decadal SSTAs, which represents variability confined to the subarctic frontal zone (Nakamura et al. 1997), clearly shows a signal extending eastward along the subarctic front from the east coast of Japan. Though not as significant as in the OFES SSH field shown in Fig. 12, the eastward propagation of decadal-scale anomalies along the Oyashio and subarctic fronts is also found in a Hovmöller diagram based on the JMA-SST data. In contrast, no such eastward propagating signals are apparent along the KE front. Mechanisms for the eastward propagating signals are not clear and there is a possibility that they are westward-propagating Rossby waves but disrupted by some unknown processes. Further investigations are necessary for the eastward propagating signals.

5. Discussion: Possible mechanisms for the decadal variability in the KOE region simulated in the OFES

a. *Surface heat flux anomalies*

Many previous studies on decadal SST variability over the North Pacific have unveiled the particular importance of anomalous heat exchanges between the ocean and atmosphere (e.g., Cayan 1992; Lau and Nath 1994; Alexander et al. 2002). Given their large horizontal scales as apparent in a difference map of the surface wind stress (Fig. 13), atmospheric anomalies cannot directly force the strong confinement of SSTAs to narrow frontal zones, as observed and simulated in the KOE region, by changing surface heat fluxes.

In fact, as evident in Fig. 14 the net upward surface heat fluxes simulated at the surface in the subarctic and KE frontal zones are *weaker* in the cool period (1984-88) than in the warm period (1968-72). This indicates that the heat flux anomalies in the OFES simulation act to *damp,* but not force the SSTAs along the fronts, as recently observed (Tanimoto et al. 2003) and simulated

(Yasuda and Kitamura 2003) in the KOE region. Rather, decadal-scale SSTAs in the KOE region are likely generated and maintained through oceanic processes (Xie et al. 2000; Seager et al. 2001; Schneider et al. 2002; Yasuda and Kitamura 2003), and rather the SSTAs act to force the overlying atmosphere thermally (Tanimoto et al. 2003; Nakamura et al. 2004).

b. *Anomalous Ekman cooling*

Changes in the temperature advection by the surface Ekman flow can also act to induce SSTAs in frontal zones effectively. The advection should be particularly strong across the zonally oriented frontal zones in the KOE region, in the presence of the meridional Ekman transport induced by the prevailing surface westerly winds over the North Pacific in winter. For each of the five-year periods of 1968-72 and 1984-88, the Ekman advection was estimated for individual winter months separately, based on the corresponding five-year mean fields of surface wind stress and simulated SST. The advection thus estimated was then converted into its local influence on the January-March mean SST, by integrating the advection over the whole winter season (from October to March) and assuming the mean mixed layer depth to be fixed locally to its January-March mean value.

As shown in Fig. 15, changes in the Ekman advection effect thus estimated from the 1984-88 to the 1968-72 periods are pronounced in the KOE region. Despite the strongest enhancement of the surface wind stress was observed between 35°N and 40°N (Fig. 13), the strongest effect of the enhanced Ekman advection on SST is estimated along the subarctic front across which the meridional SST gradient is the tightest. It should be stressed, however, that no advective effect greater than -1.5°C is found in the KOE region, where the simulated cooling in the mixed layer shown in Fig. 4 reaches as much as -4°C. We therefore conclude that, though contributing significantly (e.g., Yasuda and Hanawa 1997), the anomalous Ekman advection can account for only a fraction of the decadal-scale SST changes simulated in the subarctic frontal zone, owing to

the deep mixed layer in late winter (Fig. 8; Tomita and Nonaka 2005)[2].

c. *Anomalous Ekman pumping and baroclinic wave propagation*

Another possible mechanism for the decadal-scale SSTAs simulated in the KOE region is the generation of baroclinic Rossby waves by the anomalous Ekman pumping and their westward propagation. Once reaching into the region, the waves can cause meridional migration of fronts, resulting in temperature anomalies confined to the vicinities of the frontal axes.

1) ALONG THE KE FRONT

In a longitude-time section along the KE front (Fig. 12 left panel), decadal-scale anomalies in the Ekman pumping are superimposed on SSH anomalies with black contours. In this section, negative (positive) SSH anomalies in the KOE region tend to follow positive (negative) Ekman pumping anomalies in the central portion of the basin (160°E~160°W) that locally act to induce the shallower (deeper) thermocline and thereby negative (positive) SSH anomalies. A close examination reveals that the SSH anomalies associated with Rossby waves tend to be intensified due to anomalous Ekman pumping on their pathways toward the western basin (c.f., Miller et al. 1998).

The propagating nature of the decadal-scale anomalies in the OFES simulation is in agreement with a modeling study by Schneider and Miller (2001), who showed that temperature variability in the KOE region could be explained mostly by the first baroclinic Rossby waves

[2] The above conclusion has been confirmed by the following evaluation. As discussed in the previous subsection, the surface heat flux acts to damp the SSTAs in the KOE region, and thus locally the decadal changes in the flux (ΔQ) may be approximated to be proportional to the corresponding change in SST (ΔT). The damping coefficient (γ) can be defined as $\gamma=\Delta Q/\Delta T$. It is then possible to estimate a local change in SSTA that would be generated solely by the decadal change in the Ekman advection (ΔT_{Ek}), by dividing the local difference in Ekman advection estimated above (ΔQ_{Ek}) by γ. The estimated values turned out to be less than -1.5°C in most of the subarctic and KE frontal zones (figure not shown). Therefore, the contribution from the anomalous Ekman advection cannot account for the major fraction of the simulated total SST differences that reach as much as -4°C (Fig. 4).

propagating from the central or eastern portions of the basin. Our result is also in agreement with Qiu (2003), who showed that SSH variability in the KOE region observed by the TOPEX/Poseidon altimeter satellite since 1992 can be explained well by Rossby wave propagation. In fact, the left panel of Fig. 12 suggests that anomalous Ekman pumping at 36°N in the 1982-86 period between 170°E and 160°W could force SSH anomalies simulated in the 1984-88 period between 150°E and 170°E[3]. The intensification and accompanying southward extension (not shown) of upward Ekman pumping and the associated Rossby waves can induce both the vertical displacement of the thermocline (Schneider and Miller 2001; Schneider et al. 2002) and the southward migration of the axis of the KE front (Seager et al. 2001), as simulated in the OFES (Figs. 8 and 9). The associated SSH anomalies are, however, confined to the frontal zone and have much smaller meridional scale than the wind forcing anomalies themselves (Fig. 13). Very recently, using a high-resolution regional OGCM, Taguchi et al. (2005) also showed that narrow anomalous jets are organized in the KOE region in response to a broad meridional scale forcing, suggesting the importance of nonlinear processes including anomalous potential vorticity advection and associated adjustment in recirculation.

2) ALONG THE SUBARCTIC FRONT

In the subarctic frontal zone (Fig. 12 right panel), decadal SSH signals are also propagating westward from the central or eastern portion of the basin to its western part. A comparison between the SSH and Ekman pumping anomaly fields suggests that their relation is consistent with the dynamical influence of Ekman pumping anomalies on the SSH anomalies in the eastern basin to the east of 160°W. In the central basin, however, they are not well correlated. Additionally, as mentioned in the preceding section, there appear to be also eastward propagating signals in the western basin, which join the westward propagating signals around 170°E. The

[3] It is noteworthy that zonal extent of significant Ekman pumping anomalies changes with time: they are confined to the central portion of the basin (160°E~160°W) in the 1950s and 1960s, but they are basin wide since the 1980s.

eastward propagating signals associated with the decadal variability in the western basin, if exist, should be caused by a mechanism other than the Rossby wave propagation. In fact, Qiu (2003, his Fig. 9) has shown that Rossby wave propagation cannot explain the SSH variability in the subarctic frontal zone near the western boundary. While the importance of the variability in the subarctic front for inducing decadal SSTAs has been shown in this study, the variability cannot be fully explained by conventional mechanisms and thus further investigations are necessary.

6. Summary

Analyzing the output of a hindcast integration of an eddy-resolving quasi-global OGCM (OFES), we have investigated decadal-scale variability of the KE, Oyashio and subarctic fronts and associated temperature, salinity and SSH fluctuations in the KOE region. We have confirmed that the OFES can resolve the meridional separation between the KE and subarctic fronts along the extensions of the Kuroshio and Oyashio currents, respectively (Figs. 1, and 2), as revealed by satellite measurements, and the distinctive vertical structure of the fronts as well. We have also confirmed that gross features of decadal-scale SST variability in the KOE region are also well reproduced, as already revealed from ship and satellite measurements (Figs. 3, and 4). Thus, the 50-year OFES simulation gives us the first opportunity to study the decadal variability in the three-dimensional structure of the fronts in the KOE region.

The decadal-scale SST and SSH changes in the KOE region as extracted in a difference field between the two five-year periods of 1984-88 and 1968-72 are confined mainly to the zonally-oriented narrow frontal zones (Fig. 4), in association with the decadal-scale southward migration of their axes and the intensification of the fronts and associated currents (Figs. 5, 6, and 7). For each of the KE and subarctic fronts, the migration of the axis and associated temperature and salinity anomalies are not confined to the surface layer but extending downward into subsurface layers. The vertical extent of the anomalies, however, differs substantially between the

two fronts, reflecting their distinctive vertical structures (Fig. 8). The temperature and salinity anomalies associated with the subarctic front have their vertical maxima in the surface mixed layer, whereas they are deep and maximized in the subsurface layer (300~400 m below the surface) along the KE front (Fig. 8). In the OFES simulation, the decadal-scale southward migration of the subarctic front is more or less uniform along its zonally-oriented axis, while that of the KE front tends to be enhanced eastward along its axis in association with the change from its SW-NE orientation to its more zonal orientation.

The decadal-scale intensification of the KE current and associated front accompanies upward displacement of the thermocline and significant cooling just to the north of the frontal axis, as observed (Figs. 7 and 9). Obviously, the cooling cannot be explained by the enhanced warm water advection due to the intensified KE current. In contrast, the enhanced cool advection by the intensified Oyashio (extension) current can contribute to the decadal-scale cooling in the subarctic frontal zone, at least in the OFES simulation, although assessing the significance of this advective effect is beyond the scope of the present study.

The decadal-scale changes in the frontal axis and intensity below the surface are maintained in summer under the shallow seasonal thermocline, as they are shielded from the atmospheric thermal influence. The associated temperature anomalies in the subsurface layer are also retained in summer until they possibly re-emerge up to the surface by the following winter (Fig. 11). The seasonal persistency of the subsurface thermal anomalies in the frontal zones suggests that, in addition to the conventional re-emergence mechanism for subsurface thermal anomalies associated with the seasonal deepening of the surface mixed layer (so-called “Namias-Born mechanism”), another kind of re-emergence mechanism may be operative in the KOE region, which is associated with frontal anomalies due to ocean dynamics.

In the OFES simulation, time evolution of the decadal-scale anomalies in temperature, salinity (Fig. 8) and SSH (Fig. 12) exhibits a tendency that the changes in the subarctic frontal

zone slightly precede those in the KE frontal zone. This time lag seems to be attributable, in part, to the differences between Ekman pumping anomalies forced in the two frontal zones (Fig. 12). The anomalous Ekman pumping induces and reinforces baroclinic Rossby waves that propagate westward along each of the frontal zones. The associated anomalies with westward propagation and intensification are prevailing in the SSH variability along each of the frontal zones. Additionally, longitude-time sections suggest that there appear to be eastward propagating signals as well as the westward propagating ones along the subarctic front, while only the latter can be found at the KE front (Fig. 12).

While mechanisms for the changes documented in this study have not been investigated in depth, the difference in the anomaly evolution between the two fronts suggests that different mechanisms may be operative in causing their distinctive variability. In the KE front region, the decadal variability is largely explained by the westward propagation of the baroclinic Rossby waves forced by large-scale Ekman pumping anomalies in the central North Pacific. Those in the subarctic front region, however, cannot be fully understood with the conventional mechanisms only. Despite these distinctive structures and anomaly evolution between the two frontal zones in the KOE region, the decadal variability in the entire KOE region as a whole was regarded as a unified phenomenon in most of the previous studies. This is probably because resolutions of the observation and/or model output data were not sufficient to resolve the two fronts as separate entities, but the separation may be of some significance for the climate variability. For example, in the OFES simulation, decadal-scale SST fluctuations tend to be particularly large along the subarctic front rather than along the KE front, as already observed (Nakamura and Yamagata 1999; Nakamura and Kazmin 2003), and the same tendency is found in heat release anomalies from the ocean (Fig. 14). It is thus suggested that understanding the dynamics of the variability of the Oyashio and subpolar gyre will be of particular importance for the atmosphere-ocean coupling.

Decadal-scale SSTAs confined to the frontal zones as observed and simulated in the KOE region are manifestations of the corresponding variability of the fronts with respect to their intensities and axial positions, which are induced primarily by the ocean dynamics rather than by direct atmospheric forcing. Recent observational studies have indicated that SSTAs in the KOE region caused by the ocean dynamics can feedback to the overlying atmosphere as their influence on near surface stratification and wind profiles (Nonaka and Xie 2003; Xie 2004) and turbulent heat fluxes (Tanimoto et al. 2003). How SSTAs along such a midlatitude oceanic front as the subarctic or KE front can modify atmospheric baroclinicity and thereby storm track activity is also particular scientific significance (e.g., Tanimoto et al. 2003; Nakamura and Simpo 2004; Inatsu et al. 2003). We are planning to investigate the possible oceanic influence on the atmospheric circulation by using our high resolution atmospheric GCM on the Earth Simulator, AFES (Ohfuchi et al. 2004, 2005).

Acknowledgments.

We would like to thank members of the OFES group, including Dr. Y. Masumoto and Dr. T. Yamagata for their efforts in the model development. Our thanks are extended to Drs. S.-P. Xie, S. Minobe, N. Schneider, and Z. Liu for valuable discussions. The AMSR-E data have been produced by Remote Sensing Systems (www.remss.com) under the sponsorship of the NASA Earth Science REASon DISCOVER Project and the AMSR-E Science Team.

REFERENCES

Alexander, M. A., 1992: Midlatitude Atmosphere-Ocean interaction during El Nino. Part I: The North Pacific Ocean. *J. Climate*, **5**, 944-958.

Alexander, M. A., C. Deser, and M. S. Timlin, 1999: The Reemergence of SST anomalies in the North Pacific Ocean. *J. Climate*, **12**, 2419-2433.

Alexander, M. A., I. Blade, M. Newman, J. R. Lanzante, N. C. Lau, and J. D. Scott, 2002: The atmospheric bridge: The influence of ENSO teleconnections on air-sea interaction over the global oceans. *J. Climate*, **15**, 2205-2231.

Barnett, T. P., D. W. Pierce, R. Saravanan, N. Schneider, D. Dommenget, and M. Latif, 1999: Origins of the midlatitude Pacific decadal variability. *Geophys. Res. Lett*., **26**, 1543-1546.

Boyer, T. P., S. Levitus, J. I. Antonov, M. E. Conkright, T. O'Brien, and C. Stephens, 1998a: World Ocean Atlas 1998 Vol. 4: Salinity of the Atlantic Ocean, NOAA Atlas NESDIS 30. US Government Printing Office, Washington, D.C.

Boyer, T. P., S. Levitus, J. I. Antonov, M. E. Conkright, T. O'Brien, and C. Stephens, 1998b: World Ocean Atlas 1998 Vol. 5: Salinity of the Pacific Ocean, NOAA Atlas NESDIS 31. US Government Printing Office, Washington, D.C.

Boyer, T. P., S. Levitus, J. I. Antonov, M. E. Conkright, T. O'Brien, C. Stephens, and B. Trotsenko, 1998c: World Ocean Atlas 1998 Vol. 6: Salinity of the Indian Ocean, NOAA Atlas NESDIS 30. US Government Printing Office, Washington, D.C.

Cayan, D. R., 1992: Latent and sensible heat flux anomalies over the northern oceans: Driving the sea surface temperature. *J. Phys. Oceanogr*., **22**, 859-881.

Chelton, B. D., and M. G. Schlax, 1996: Global observations of oceanic Rossby waves. *Science*, **272**, 234-238.

Deser, C., M. A. Alexander, and M. S. Timlin, 1996: Upper-ocean thermal variations in the North Pacific during 1970-1991. *J. Climate*, **9**, 1840-1855.

Deser, C., M. A. Alexander, and M. S. Timlin, 1999: Evidence for a wind-driven intensification of the Kuroshio current extension from the 1970s to 1980s. *J. Climate*, **12**, 1697-1706.

Deser, C., M. A. Alexander, and M. S. Timlin, 2003: Understanding the persistence of sea surface temperature anomalies in midlatitudes. *J. Climate*, **16**, 57-72.

Graham, N. E., 1994: Decadal-scale climate variability in the tropical and North Pacific during the 1970's and 1980's: Observations and model result. *Clim. Dyn*., **10**, 135-162.

Inatsu, M., H. Mukougawa, and S.-P. Xie, 2003: Atmospheric response to zonal variations in midlatitude SST: Transient and stationary eddies and their feedback. *J. Climate*, **16**, 3314-3329.

Kalnay, E., et al., 1996: The NCEP/NCAR 40-year reanalysis project, *Bull. Amer. Meteor. Soc*., **77**, 437-471.

Kawamura, R., 1994: A rotated EOF analysis of global sea surface temperature variability with interannual and interdecadal scales. *J. Phys. Oceanogr*., **24**, 707-715.

Kushnir, Y., W. A. Robinson, I. Blade, N. M. J. Hall, S. Peng, and R. Sutton, 2002: Atmospheric GCM response to extratropical SST anomalies: Systhesis and evaluation. *J. Climate*, **15**, 2233-2256.

Large, W. G., J. C. McWilliams, and S.C. Doney, 1994: Oceanic vertical mixing: A review and a model with a nonlocal boundary layer parameterization, *Rev. Geophys*., **32**, 363-403.

Latif, M., and T. P. Barnett, 1994: Causes of decadal climate variability over the North Pacific and North America. *Science*, **266**, 634-637.

Lau, N. C., and M. J. Nath, 1994: A modeling study of the relative roles of tropical and extratropical SST anomalies in the variability of the global atmosphere-ocean system. *J. Climate*, **7**, 1184-1207.

Mantua, N. J., S. R. Hare, Y. Zhang, J. M. Wallace, and R. C. Francis, 1997: A Pacific interdecadal climate oscillation with impacts on salmon production. *Bull. Amer. Meteor. Soc*., **76**, 1069-1079.

Masuda, S., :Role of the ocean in the decadal climate change in the North Pacific. J. Geophys. Res., 107, 3224, doi:10.1029/2002JC001420.

Masumoto, Y., H. Sasaki, T. Kagimoto, N. Komori, A. Ishida, Y. Sasai, T. Miyama, T. Motoi, H. Mitsudera, K. Takahashi, H. Sakuma, and T. Yamagata, 2004: A Fifty-Year Eddy-Resolving Simulation of the World Ocean -Preliminary Outcomes of OFES (OGCM for the Earth Simulator)-, *The Journal of the Earth Simulator*, **1**, 31-52.

Miller, A. J., and N. Schneider, 2000: Interdecadal climate regime dynamics in the North Pacific Ocean: Theories, observations and ecosystem impacts. *Prog. Oceanogr*., **47**, 355-379.

Miller, A. J., D. R. Cayan, and W. B. White, 1998: A westward-intensified decadal change in the North Pacific thermocline and gyre-scale circulation. *J. Climate*, **11**, 3112-3127.

Mizuno, K., and W. B. White, 1983: Annual and interannual variability in the Kuroshio Current System. *J. Phys. Oceanogr*., **13**, 1847-1867.

Nakamura, H., and T. Yamagata, 1999: Recent decadal SST variability in the northwestern Pacific and associated atmospheric anomalies. *Beyond El Nino: Decadal and Interdecadal Climate Variability*, edited by A. Navarra, pp. 49-72, Springer, New York.

Nakamura, H., and A. S. Kazmin, 2003: Decadal changes in the North Pacific oceanic frontal zones as revealed in ship and satellite observations. *J. Geophys. Res*., **108**, 3078-3094.

Nakamura, H., and A. Shimpo, 2004: Seasonal variations in the Southern Hemisphere storm track and jes streams as revealed by reanalysis dataset. *J. Climate*, **17**, 1828-1844.

Nakamura, H., G. Lin, and T. Yamagata, 1997: Decadal climate variability in the North Pacific during the recent decades. *Bull. Amer. Meteor. Soc*., **78**, 2215-2225.

Nakamura, H., T. Sampe, Y. Tanimoto, and A. Shimpo, 2004: Observed associations among storm

tracks, jet streams and midlatitude oceanic fronts. In *Earth Climate: The Ocean-Atmosphere Interaction*, C. Wang, S.-P. Xie, and J.A. Carton (eds.), Geophysical Monograph, 147, AGU, Washington D.C., 329-345.

Namias, J., and R. M. Born, 1974: Further studies of temporal coherence in North Pacific sea surface temperatures. *J. Geophys. Res*., **79**, 797-798.

Newman, M., G. P. Compo, and M. A. Alexander, 2003: ENSO-forced variability of the Pacific Decadal Oscillation. *J. Climate*, **16**, 3853-3857.

Nitta, T., and S. Yamada, 1989: Recent warming of tropical sea surface temperature and its relationship to the Northern Hemisphere circulation. *J. Meteor. Soc. Jpn*., **67**, 375-382.

Nonaka, M., and S.-P. Xie, 2003: Covariations of sea surface temperature and wind over the Kuroshio and its extension: Evidence for ocean-to-atmosphere feedback. *J. Climate*, **16**, 1404-1413.

Norris, J. R., Y. Zhang, and J. M. Wallace, 1998: Role of low clouds in summertime atmosphere-ocean interactions over the North Pacific. *J. Climate*, **11**, 2482-2490.

Ohfuchi, W., S. Shingu, H. Nakamura, M. K. Yoshioka, T. Enomoto, K. Takaya, S. Yamane, T. Nishimura, X. Peng, H. Fuchigami, M. Yamada, Y. Kurihara, and K. Ninomiya, 2004: 10-km mesh meso-scale resolving simulations of the global atmosphere on the Earth Simulator - Preliminary outcomes of AFES (AGCM for the Earth Simulator). *The Journal of the Earth Simulator*, **1**, 8-34.

Ohfuchi, W., H. Sasaki, Y. Masumoto, and H. Nakamura, 2005: Meso-scale resolving simulations of the global atmosphere and ocean on the Earth Simulator. *EOS trans*., **86**, 45-46.

Pacanowski R. C., and S. M. Griffies, 2000: MOM 3.0 Manual, Geophysical Fluid Dynamics Laboratory/National Oceanic and Atmospheric Administration, 680pp.

Pierce, D. W., T. P. Barnett, N. Schneider, R. Saravanan, D. Dommenget, and M. Latif, 2001: The role of ocean dynamics in producing decadal climate variability in the North Pacific. *Clim. Dyn*. **18**, 51-70.

Qiu, B., 2000: Interannual variability of the Kuroshio Extension system and its impact on the wintertime SST field. *J. Phys. Oceanogr*., **30**, 1486-1502.

Qiu, B., 2003: Kuroshio Extension variability and forcing for the Pacific decadal oscillations: Responses and potential feedback. *J. Phys. Oceanogr*., **33**, 2465-2482.

Rosati, A., and K. Miyakoda, 1988: A general circulation model for upper ocean circulation. *J. Phys. Oceanogr*., **18**, 1601-1626.

Schneider, N., and A. J. Miller, 2001: Predicting western North Pacific oceano climate. *J. Climate*, **14**, 3997-4002.

Schneider, N., and B.D. Cornuelle, 2005: The forcing of the Pacific Decadal Oscillation. *J. Climate*, in press.

Schneider, N., A. J. Miller, and D. W. Pierce, 2002: Anatomy of North Pacific decadal variability.

J. Climate, **15**, 586-605.

Seager R., Y. Kushnir, N. H. Naik, M. A. Cane, and J. Miller, 2001: Wind-driven shifts in the latitude of the Kuroshio-Oyashio extension and generation of SST anomalies on decadal timescales. *J. Climate*, **14**, 4149-4165.

Smith, R. D., M. E. Maltrud, F. O. Bryan, and M. W. Hecht, 2000: Numerical simulation of the North Atlantic Ocean at 1/10°., *J. Phys. Oceanogr*., **30**, 1532-1561.

Stephens, C., J. I. Anntonov, T. P. Boyer, M. E. Conkright, R. A. Locarnini, T. D. O'Brien, and H. E. Garcia, 2002: World Ocean Atlas 2001, Vol. 1: Temperature. S. Levitus, Ed., NOAA Atlas NESDIS 49, US. Government Printing Office, Wash., D. C., 167 pp., CD-ROMs.

Taguchi, B., S.-P. Xie, H. Mitsudera, and A. Kubokawa, 2005: Response of the Kuroshio Extension to Rossby waves associated with the 1970s climate regime shift in a high-resolution ocean model. *J. Climate*, in press.

Tanimoto, Y., and S.-P. Xie, 2002: Inter-hemispheric decadal variations in SST, surface wind, heat flux and cloud cover over the Atlantic Ocean. *J. Meteor. Soc. Jpn*., **80**, 1199-1219.

Tanimoto, Y., N. Iwasaka, K. Hanawa, and Y. Toba, 1993: Characteristic variation of sea surface temperature with multiple time scale in the North Pacific. *J. Climate*, **6**, 1153-1160.

Tanimoto, Y., N. Iwasaka, and K. Hanawa, 1997: Relationship between sea surface temperature, the atmospheric circulation and air-sea fluxes on multiple time scales. *J. Meteorol. Soc. Jpn*., **75**, 831-849.

Tanimoto, Y., H. Nakamura, T. Kagimoto, and S. Yamane, 2003: An active role of extratropical sea surface temperature anomalies in determining anomalous turbulent heat flux. *J. Geophys. Res*., **108** (C10), 3304, doi:10.1029/2002JC001750.

Tomita, T., and M. Nonaka, 2005: Effects of mixed layer depth on wintertime sea surface temperature variability. *J. Climate*, in press.

Tomita, T., S.-P. Xie, and M. Nonaka , 2002: Estimates of Surface and Subsurface Forcing for Decadal Sea Surface Temperature Variability in the Mid-Latitude North Pacific. *J. Meteor. Soc. Jpn*, **80**, 1289-1300.

Tomita, T., B. Wang, T. Yasunari, and H. Nakamura, 2001: Spatiotemporal structure of decadal scale variability observed in the global sea surface temperature and lower-troposphere circulation fields. *J. Geophys. Res*., **106**, 26805-26815.

Trenberth, K. E., 1990: Recent observed interdecadal climate changes in the Northern Hemisphere. *Bull. Amer. Meteor. Soc*., **71**, 988-993.

Trenberth, K. E., and J. W. Hurrell, 1994: Decadal atmosphere-ocean variations in the Pacific. *Clim. Dyn*., **9**, 303-319.

White, W.B., 1995: Design of a global observing system for gyre-scale upper ocean temperature variability. *Prog. Oceanogr*., **36**, 169-217.

Woodruff, S. D., R. J. Sluts, R. L. Jenne, and P. M. Steurer, 1987: A comprehensive

ocean-atmosphere dataset. *Bull. Amer. Meteor. Soc*., **68**, 521-527.

Xie, S.-P., 2004: Satellite observations of cool ocean-atmosphere interaction. *Bull. Amer. Metor. Soc*., **85**, 195-208.

Xie, S.-P., T. Kunutani, A. Kubokawa, M. Nonaka, and S. Hosoda, 2000: Intedecadal thermocline variability in the North Pacific for 1958-1997: A GCM simulation. *J. Phys. Oceanogr*., **30**, 2798-2813.

Yasuda, I., K. Okuda, and Y. Shimizu, 1996: Distribution and modification of North Pacific Intermediate Water in the Kuroshio-Oyashio interfrontal zone. *J. Phys. Oceanogr*., **26**, 448-465.

Yasuda, T., and K. Hanawa, 1997: Decadal changes in the mode waters in the midlatitude North Pacific. *J. Phys. Oceanogr*., **27**, 858-870.

Yasuda, T., and Y. Kitamura, 2003: Long-term variability of North Pacific subtropical mode water in response to spin-up of the subtropical gyre. *J. Oceanogr*., **59**, 279-290.

Yuan, X., and L. D. Talley, 1996: The subarctic frontal zone in the North Pacific: Characteristics of frontal structure from climatological data and synoptic surveys. *J. Geophys. Res*., **101**, 16491-16508.

Zhang, Y., J. M. Wallace, and D. S. Battisti, 1997: ENSO-like interdecadal variability: 1900-1993. *J. Climate*, **10**, 1004-1020.

Figure captions

Figure 1. Monthly mean SST in the KOE region for January 2003 based on (top) the OFES simulation and (bottom) the AMSR-E observation. Contour intervals are 1°C.

Figure 2. Latitude-depth sections of climatological-mean January-March temperature averaged between 145°E and 160°E, based on the (left) OFES simulation and (right) the observation (WOA2001). Contour intervals for temperature fields are 1°C. In the right panel, meridional temperature gradient (°C/100km) is superimposed with shading (as indicated at the bottom) to indicate the KE and subarctic frontal zone.

Figure 3. Time series of regional mean wintertime (January-March) SST and subsurface temperature averaged in the KOE region [140°E-170°E, 35°N-43°N]. (Top) SST anomalies based on the OFES simulation (solid), FRS-COADS data (dashed), and hydrographic observations compiled by White (1995) (dotted). (Middle) Temperature anomalies at the sea surface, 120-, 200-, 300-, and 400-m depth based on the OFES simulation. (Bottom) The same as the middle panel except for the White's temperature data. Five-year running mean is applied to the all time series. Line types for the individual time series are shown in each panel.

Figure 4. Wintertime (January-March) mean SST fields over the North Pacific based on (top) the observation (FRS-COADS) and (bottom) the OFES simulation. Contours indicate the five-winter mean for 1984-88 (every 1°C), and color shading indicates the difference of that mean field from another five-winter mean for 1968-72, as indicated to the right of the top panel.

Figure 5. Magnitude of horizontal gradient of five-winter (January-March) mean SST for (top) 1984-88 and (bottom) 1968-72, based on the OFES simulation. Contour intervals are 0.5°C/100km, with values of 1.5 °C/100km or greater are plotted. Warm (cold) colors indicate stronger (weaker) gradients. Gray shading in the bottom panel indicates the same field as in the top panel for comparison, as indicated to the right of the bottom panel.

Figure 6. Magnitude of horizontal gradient of five-winter (January-March) mean SSH for (top) 1984-88 and (bottom) 1968-72, based on the OFES simulation. Contours for 10-, 15-, 20-, 25-, 30-, 40-cm/100km are plotted. Warm (cold) colors indicate stronger (weaker) gradients. Gray shading in the bottom panel indicates the same field as in the top panel for comparison, as indicated to the right of the bottom panel.

Figure 7. Current vectors in the surface layer and their magnitudes (shading; as indicated to the right of the panels), based on the OFES simulation averaged over the five winters (January-March) separately for (top) 1984-88 and (bottom) 1968-72. The scaling for the vectors (unit: cm s^{-1}) is indicated near the upper-left corner of each panel.

Figure 8. Latitude-depth sections of five-winter (January-March) mean (left) temperature and (right) salinity fields for the (top) 1968-72, (middle) 1976-80, and (bottom) 1984-88 periods averaged between 145°E and 160°E based on the OFES simulation. Contour intervals are 1°C (0.1 PSU) for temperature (salinity) fields. The corresponding anomalies from their 1950-2003 climatologies are plotted with color shading, as indicated below the bottom panels.

Figure 9. Latitude-depth sections of five-winter (January-March) mean fields of temperature (black contours) and its meridional gradient (color shading; as indicated to the right of the upper-right panel) for (top) 1984-88 and (middle) 1968-72. Based on their averages between 145°E and 160°E for (left) the OFES simulation and (right) hydrographic observations compiled by White (1995). Color shadings in the bottom panels indicate the changes in five-winter mean temperature from 1968-72 to 1984-88, as indicated to the right of the lower-right panel. Contour intervals for temperature are 1°C. Unit for the gradients is °C/100km.

Figure 10. As in Fig. 4 but for the summertime (July-September) mean fields.

Figure 11. Five-year mean (1984-88) temperature fields simulated at 150-m depth in the OFES for (top) winter (January-March) and (bottom) summer (July-September). Contour intervals are 1°C. Color shading indicates their difference from another five-year mean fields for 1968-72 for the respective seasons, as indicated to the right of the bottom panel.

Figure 12. Longitude-time sections of anomalies of SSH (color shading as indicated to the right of the figure; unit: cm) and Ekman pumping (black contours for ±0.25, 0.5, 1.0, 1.5 x10^{-4} cm s^{-1}; dashed for negative values) at (left) 36°N and (right) 43°N. 13-month and five-year running means have applied to the SSH and Ekman pumping anomalies, respectively, and their linear trends have been removed. A thick black line plotted in each of the panels indicates the theoretical propagating speed of the first baroclinic Rossby waves for each of the latitudes. Thick white lines are plotted in the right panel for tracing possible vestiges of eastward-propagating signals.

Figure 13. Sea surface wind-stress vectors and its magnitudes (contour intervals: 0.2 dyn cm^{-2}), which forced the OFES simulation, averaged over the five winters (January-March) separately for (middle) 1984-88 and (bottom) 1968-72. The scaling for the vectors (unit: dyn cm^{-2}) is indicated near the upper-left corner of each panel. The difference fields from the earlier period to the later are indicated in the top panel.

Figure 14. Mean difference map of the net upward heat flux at the surface from five-year period 1968-72 to another five-year period 1984-88. Contour intervals are 50 (W m^{-2}), and negative values are dashed (zero lines are omitted). Based on the OFES simulation for winter (January-March).

Figure 15. Contribution of changes in the surface Ekman advection induced by the corresponding changes in the wind stress to the SST differences between 1984-88 and 1968-72, based on the OFES simulation. For each of the five-year periods, the contribution has been evaluated locally as the mean January-March SST difference due solely to the five-year mean Ekman transport anomaly acting on the same five-year mean SST both for the whole winter season (October through March), by assuming the mixed layer depth to be fixed to its January-March mean value during the particular five-year period. The difference in the contributions estimated as above is plotted for every 0.25°C with heavy lines for every 0.5°C. Negative (i.e., enhanced cooling) values are solid, and the zero contours are omitted.

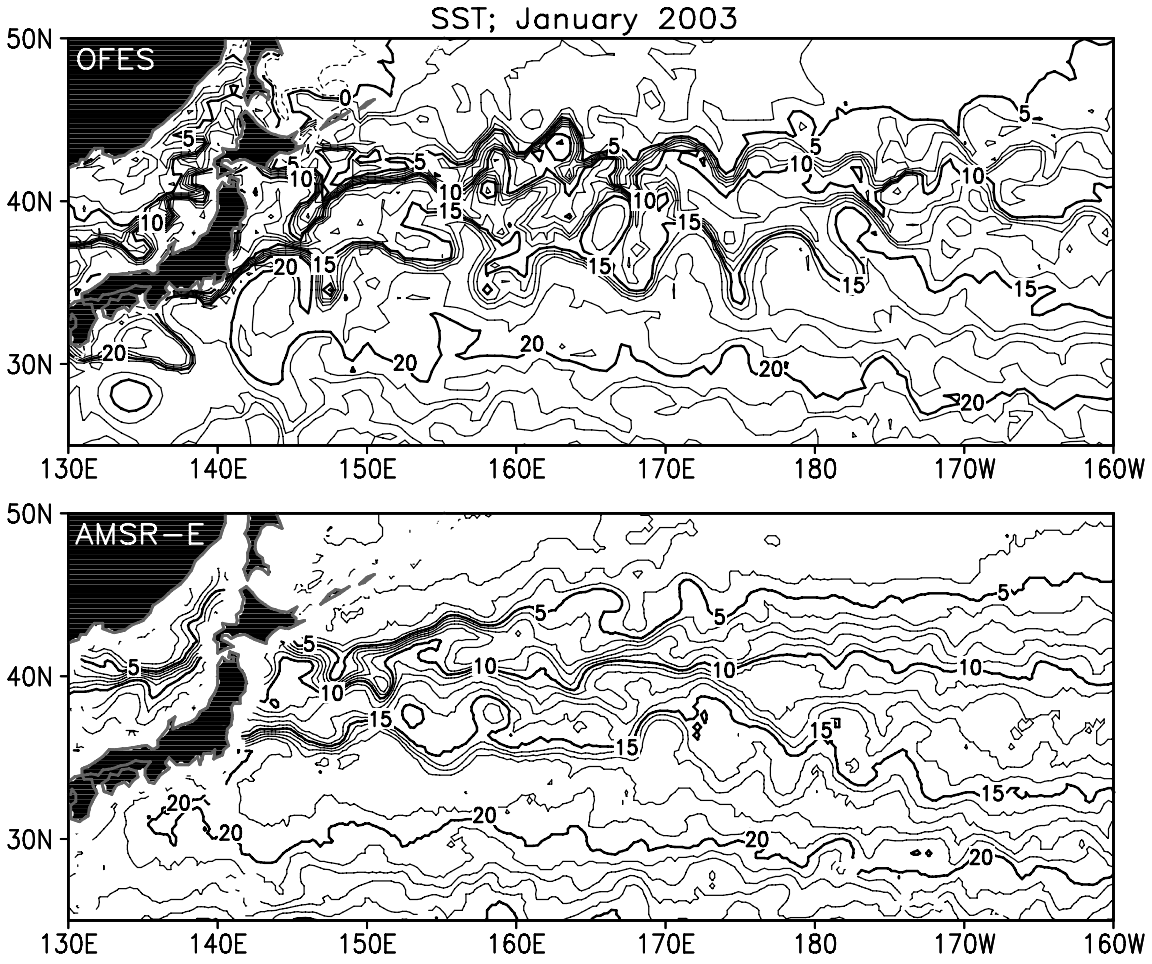

Figure 1. Monthly mean SST in the KOE region for January 2003 based on (top) the OFES simulation and (bottom) the AMSR-E observation. Contour intervals are 1°C.

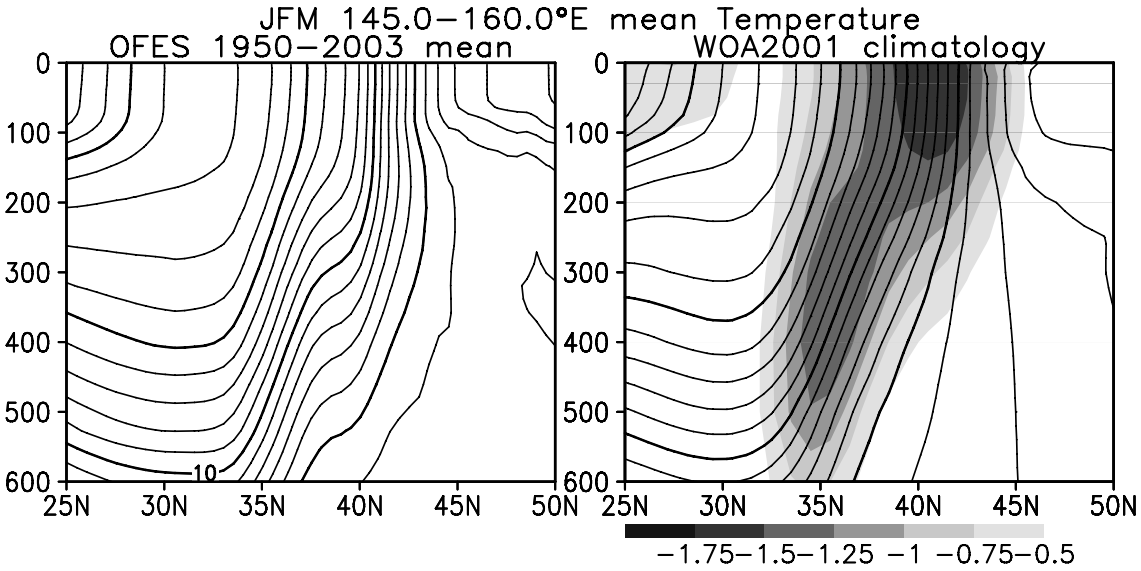

Figure 2. Latitude-depth sections of climatological-mean January-March temperature averaged between 145°E and 160°E, based on the (left) OFES simulation and (right) the observation (WOA2001). Contour intervals for temperature fields are 1°C. In the right panel, meridional temperature gradient (°C/100km) is superimposed with shading (as indicated at the bottom) to indicate the KE and subarctic frontal zone.

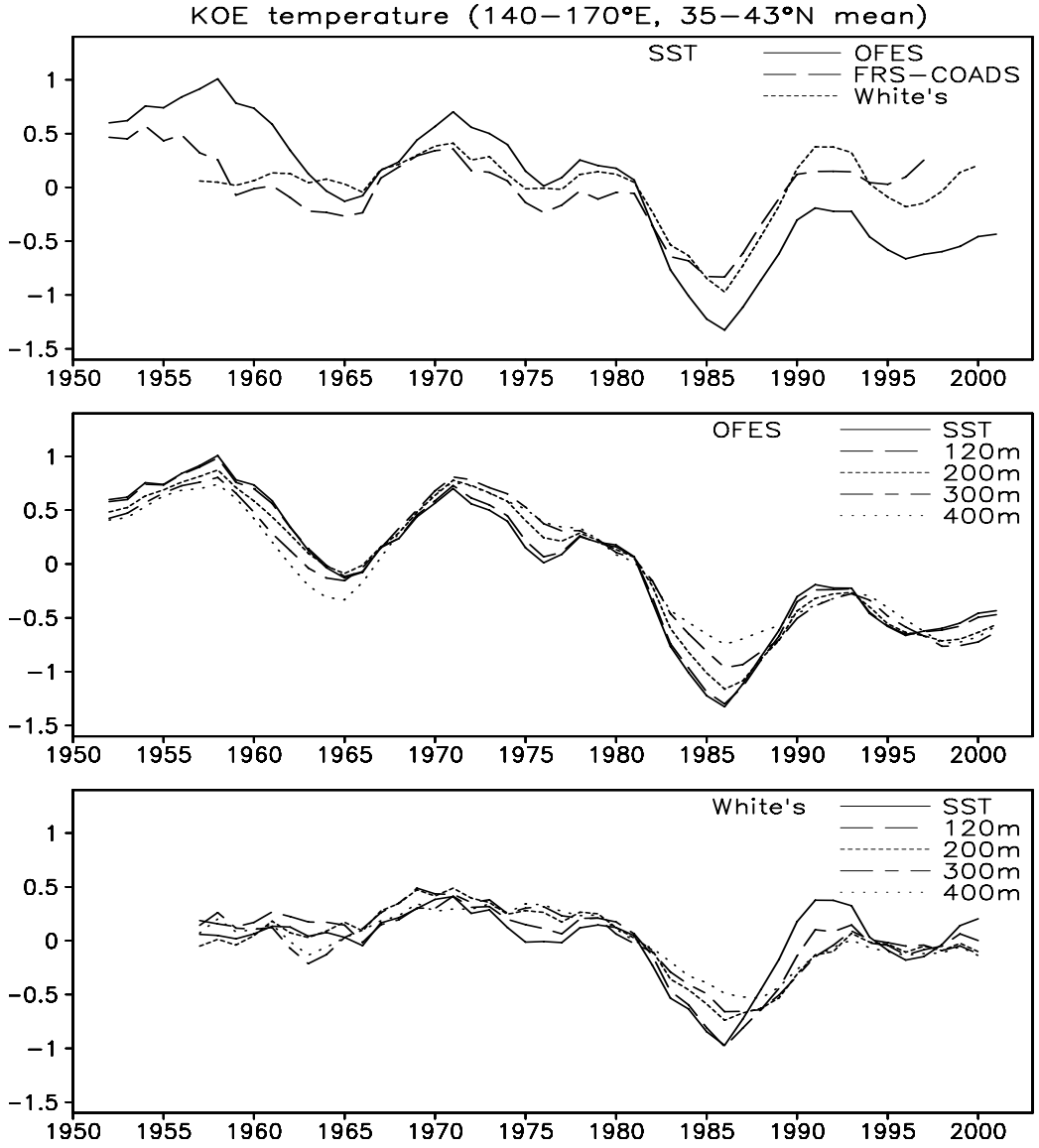

Figure 3. Time series of regional mean wintertime (January-March) SST and subsurface temperature averaged in the KOE region [140°E-170°E, 35°N-43°N]. (Top) SST anomalies based on the OFES simulation (solid), FRS-COADS data (dashed), and hydrographic observations compiled by White (1995) (dotted). (Middle) Temperature anomalies at the sea surface, 120-, 200-, 300-, and 400-m depth based on the OFES simulation. (Bottom) The same as the middle panel except for the White's temperature data. Five-year running mean is applied to the all time series. Line types for the individual time series are shown in each panel.

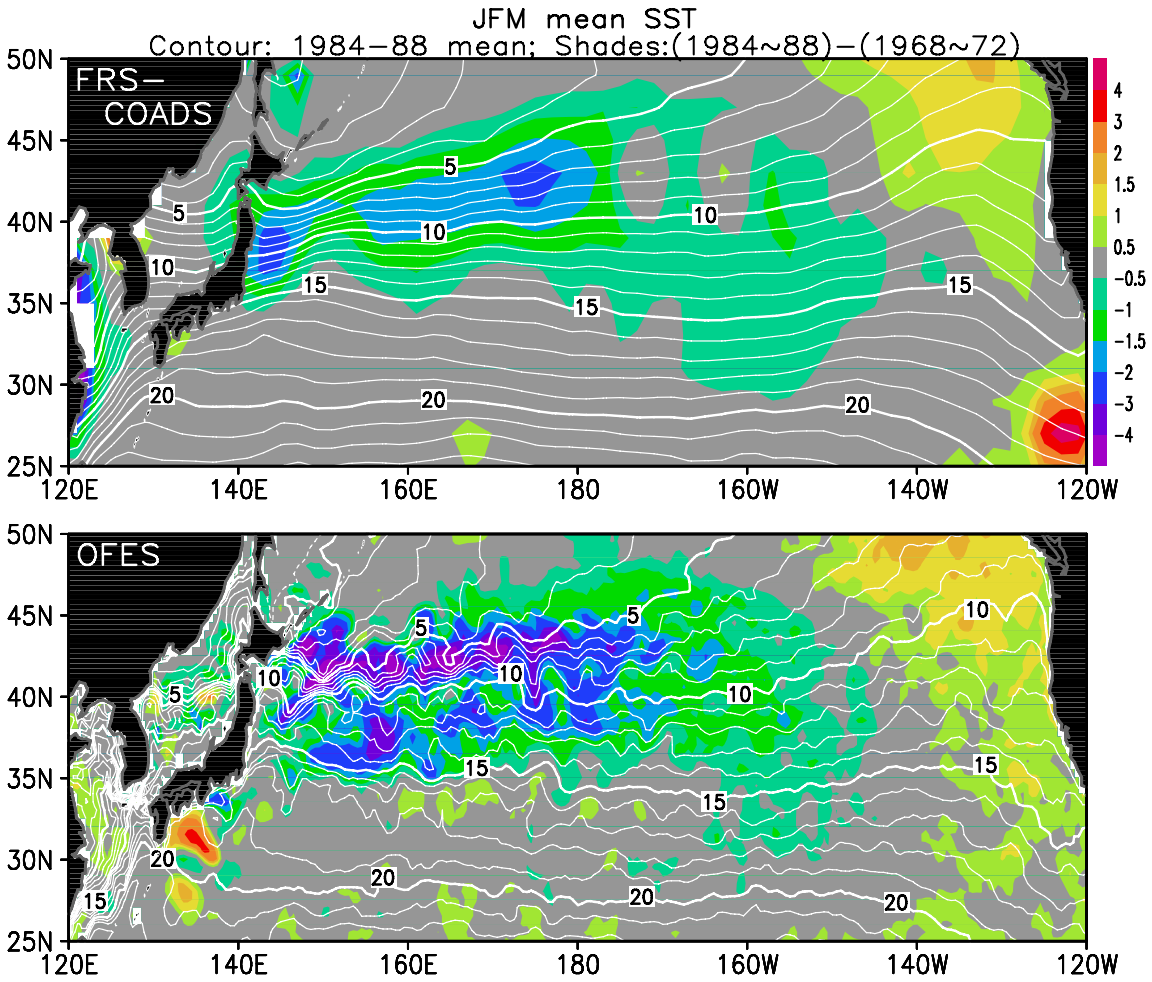

Figure 4. Wintertime (January-March) mean SST fields over the North Pacific based on (top) the observation (FRS-COADS) and (bottom) the OFES simulation. Contours indicate the five-winter mean for 1984-88 (every 1°C), and color shading indicates the difference of that mean field from another five-winter mean for 1968-72, as indicated to the right of the top panel.

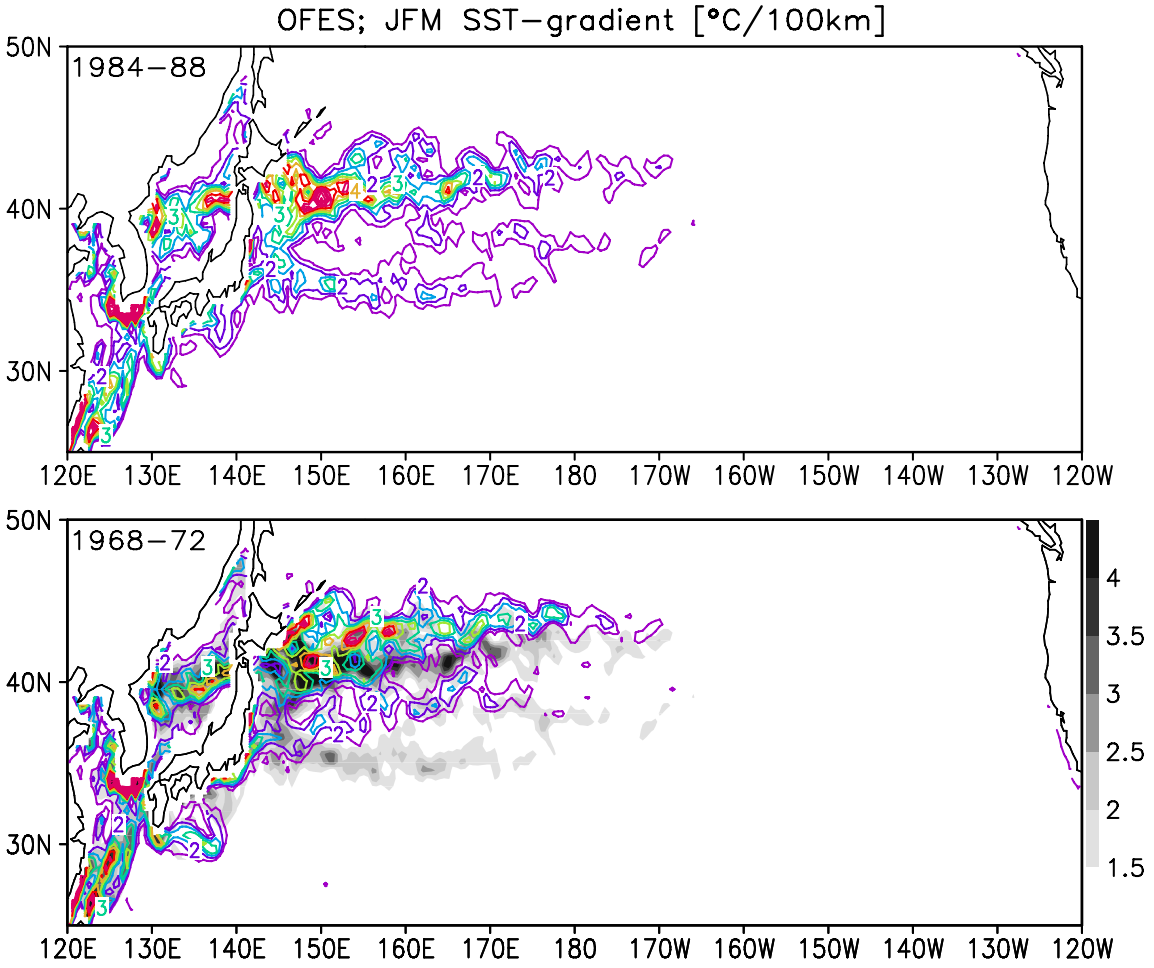

Figure 5. Magnitude of horizontal gradient of five-winter (January-March) mean SST for (top) 1984-88 and (bottom) 1968-72, based on the OFES simulation. Contour intervals are 0.5°C/100km, with values of 1.5 °C/100km or greater are plotted. Warm (cold) colors indicate stronger (weaker) gradients. Gray shading in the bottom panel indicates the same field as in the top panel for comparison, as indicated to the right of the bottom panel.

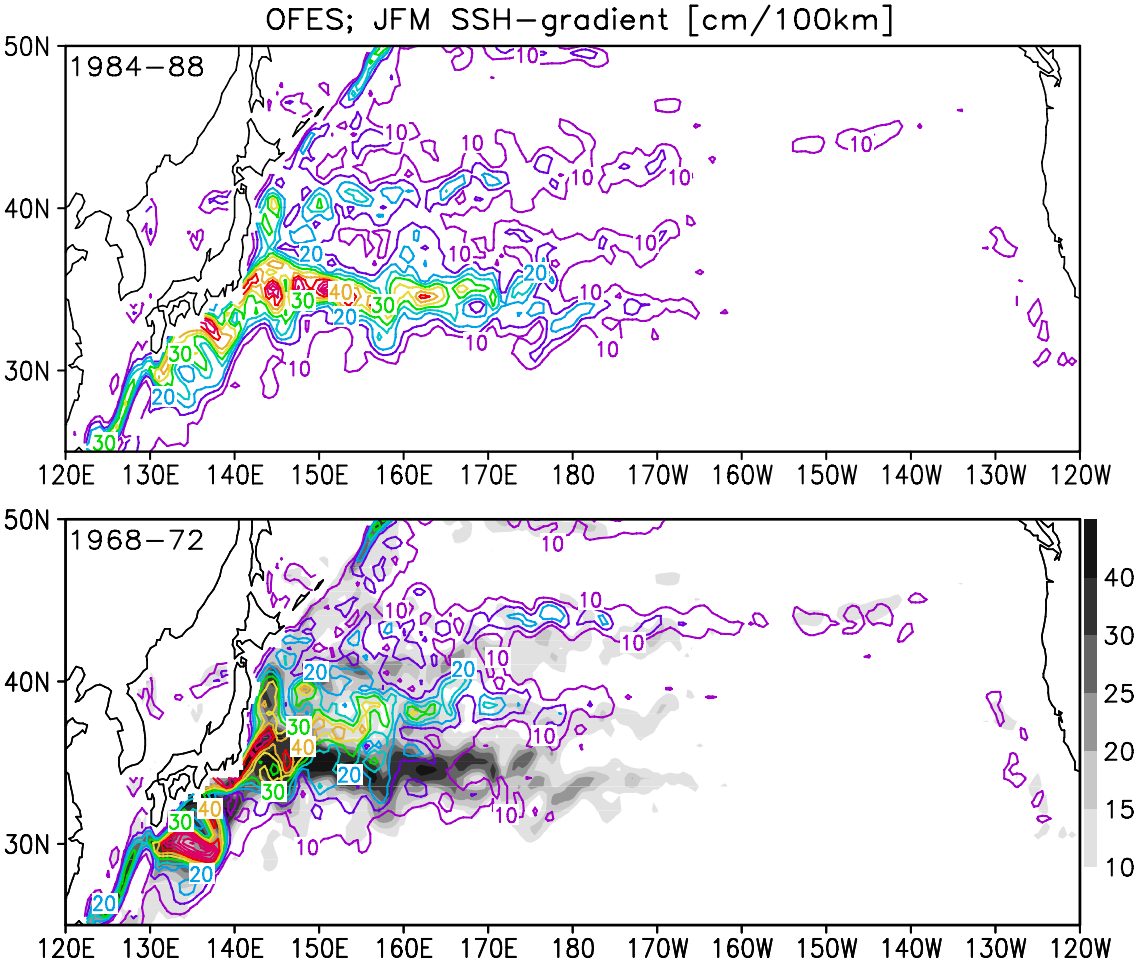

Figure 6. Magnitude of horizontal gradient of five-winter (January-March) mean SSH for (top) 1984-88 and (bottom) 1968-72, based on the OFES simulation. Contours for 10-, 15-, 20-, 25-, 30-, 40-cm/100km are plotted. Warm (cold) colors indicate stronger (weaker) gradients. Gray shading in the bottom panel indicates the same field as in the top panel for comparison, as indicated to the right of the bottom panel.

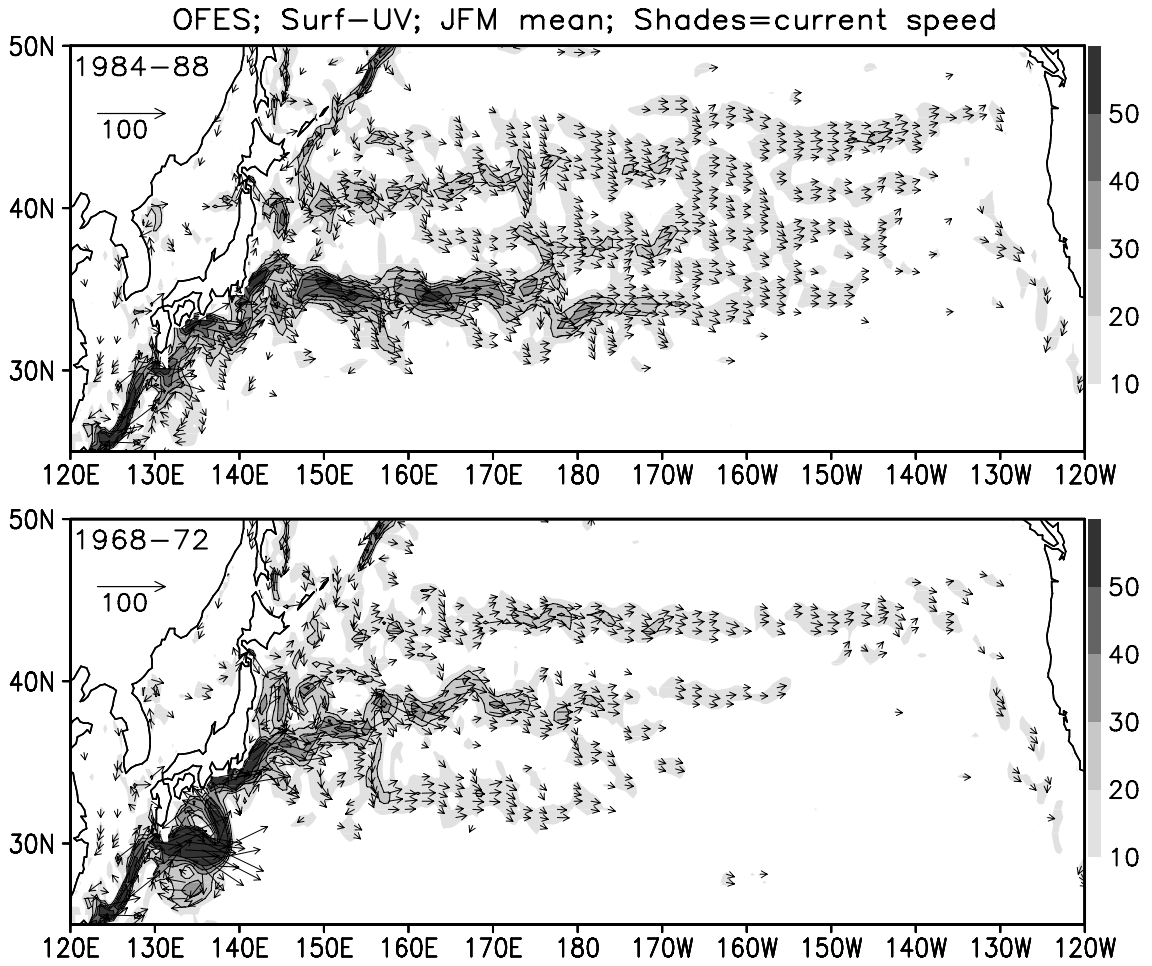

Figure 7. Current vectors in the surface layer and their magnitudes (shading; as indicated to the right of the panels), based on the OFES simulation averaged over the five winters (January-March) separately for (top) 1984-88 and (bottom) 1968-72. The scaling for the vectors (unit: cm s^{-1}) is indicated near the upper-left corner of each panel.

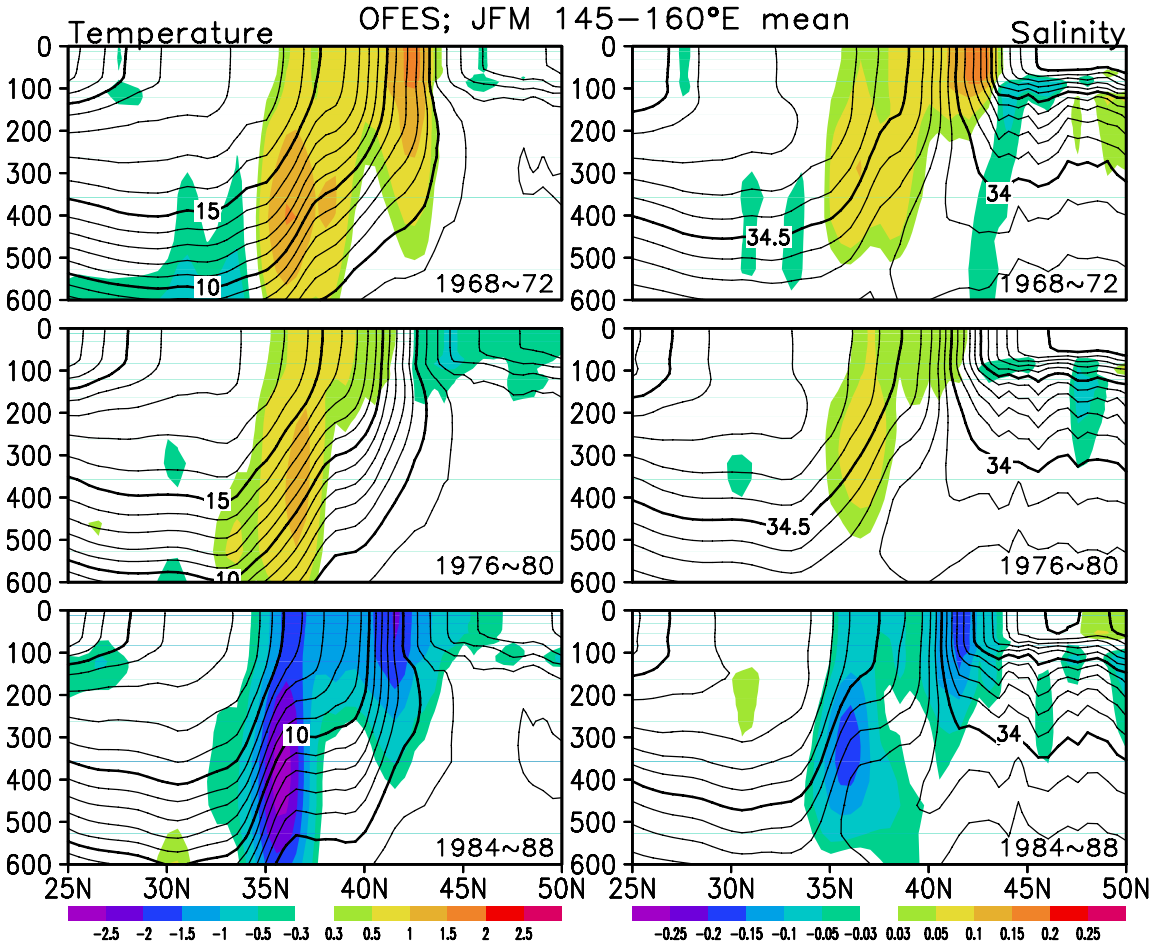

Figure 8. Latitude-depth sections of five-winter (January-March) mean (left) temperature and (right) salinity fields for the (top) 1968-72, (middle) 1976-80, and (bottom) 1984-88 periods averaged between 145°E and 160°E based on the OFES simulation. Contour intervals are 1°C (0.1 PSU) for temperature (salinity) fields. The corresponding anomalies from their 1950-2003 climatologies are plotted with color shading, as indicated below the bottom panels.

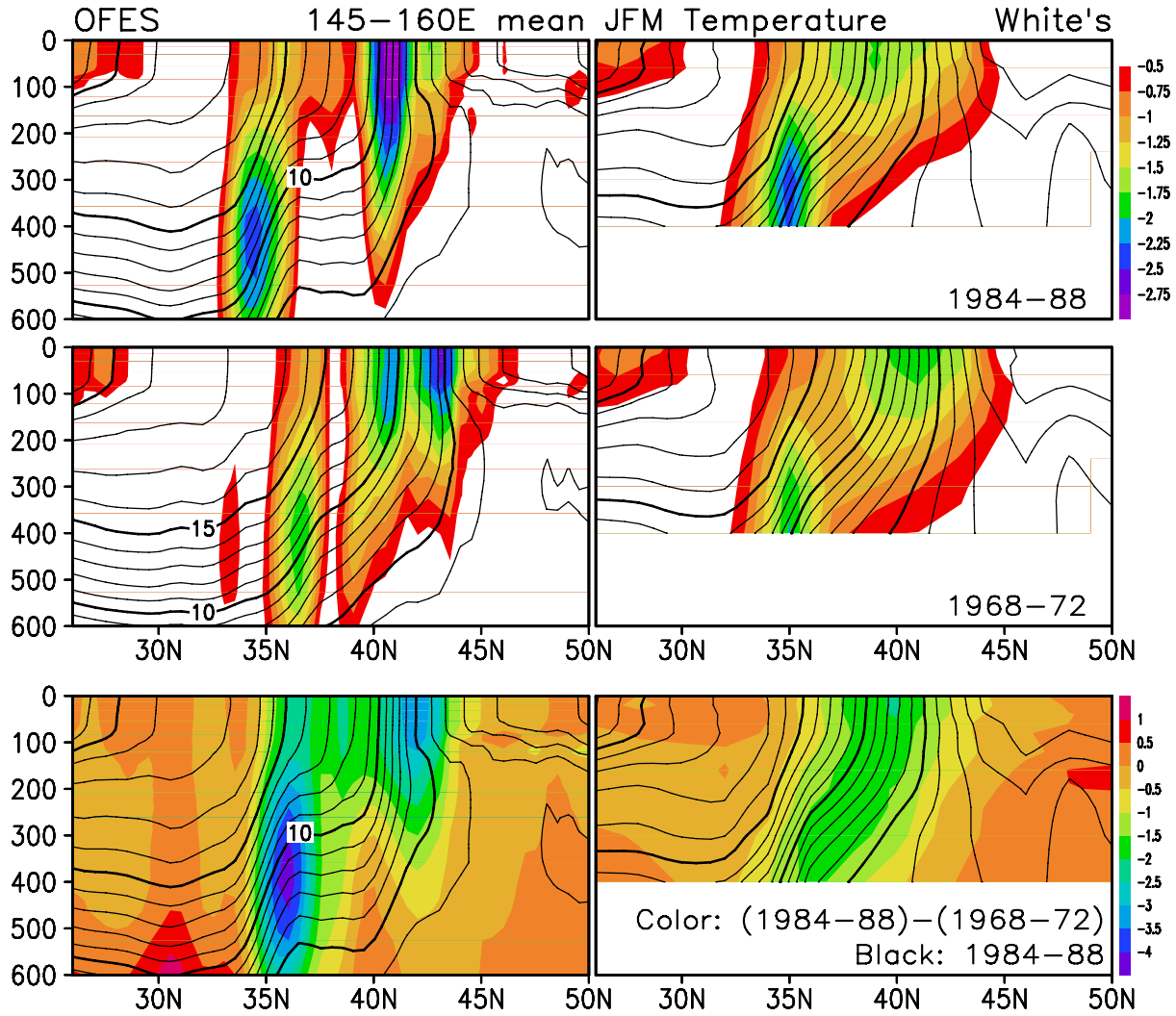

Figure 9. Latitude-depth sections of five-winter (January-March) mean fields of temperature (black contours) and its meridional gradient (color shading; as indicated to the right of the upper-right panel) for (top) 1984-88 and (middle) 1968-72. Based on their averages between 145°E and 160°E for (left) the OFES simulation and (right) hydrographic observations compiled by White (1995). Color shadings in the bottom panels indicate the changes in five-winter mean temperature from 1968-72 to 1984-88, as indicated to the right of the lower-right panel. Contour intervals for temperature are 1°C. Unit for the gradients is °C/100km.

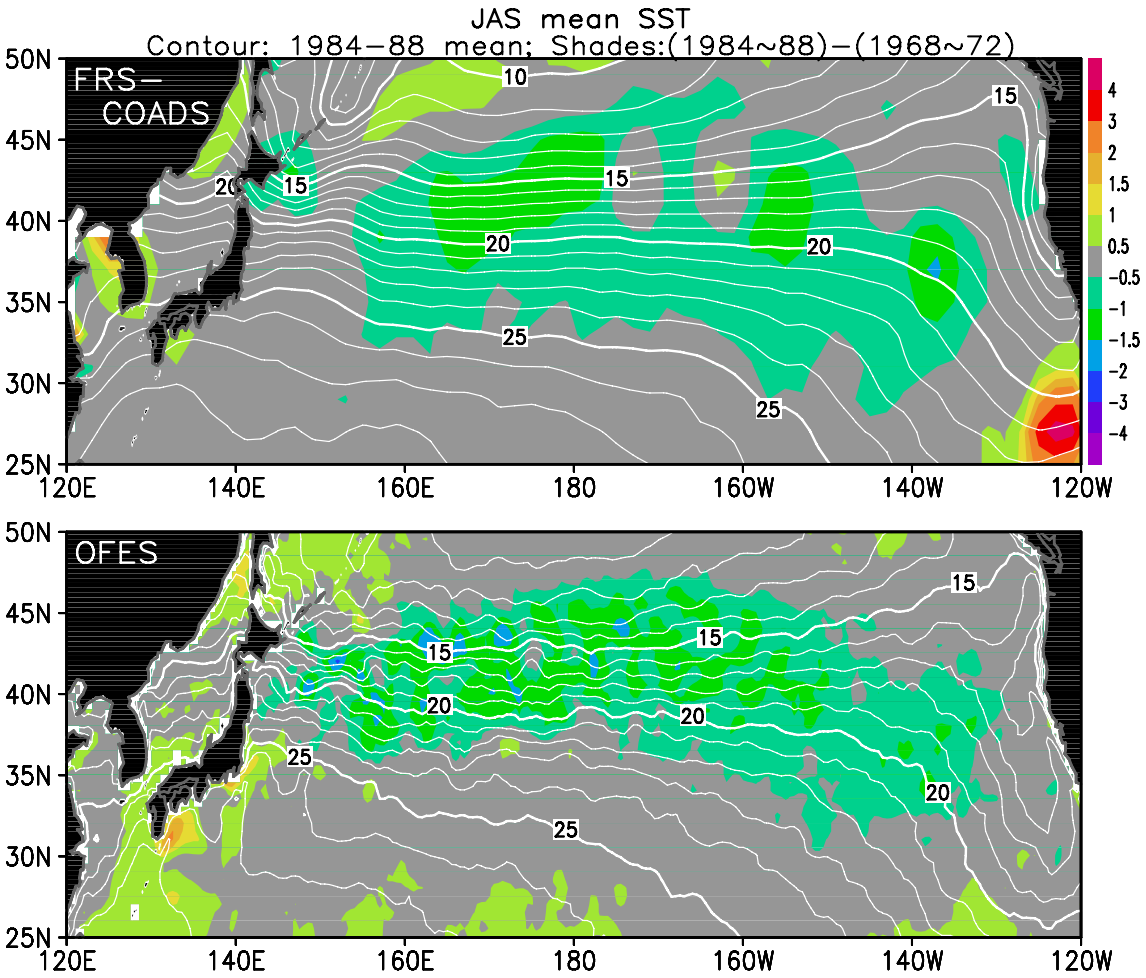

Figure 10. As in Fig. 4 but for the summertime (July-September) mean fields.

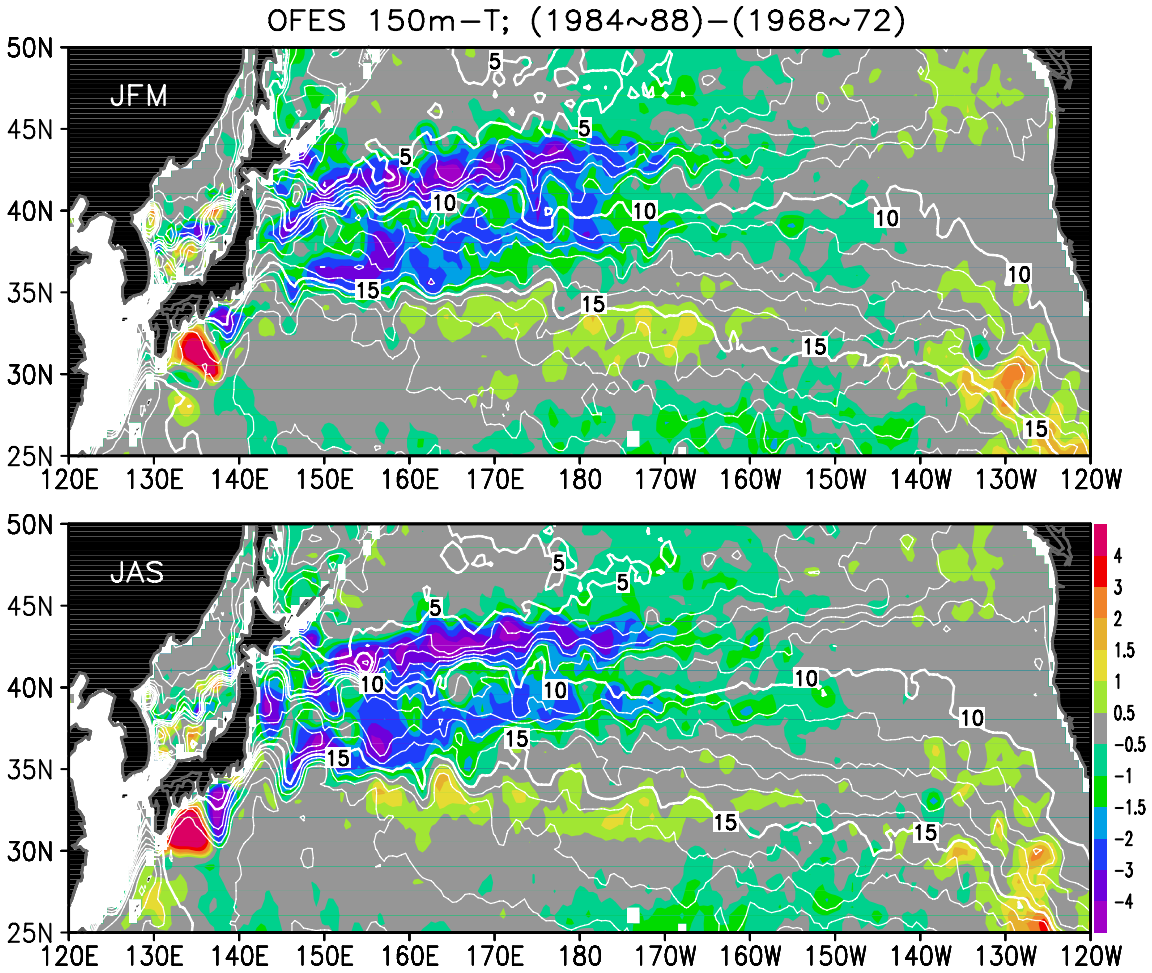

Figure 11. Five-year mean (1984-88) temperature fields simulated at 150-m depth in the OFES for (top) winter (January-March) and (bottom) summer (July-September). Contour intervals are 1°C. Color shading indicates their difference from another five-year mean fields for 1968-72 for the respective seasons, as indicated to the right of the bottom panel.

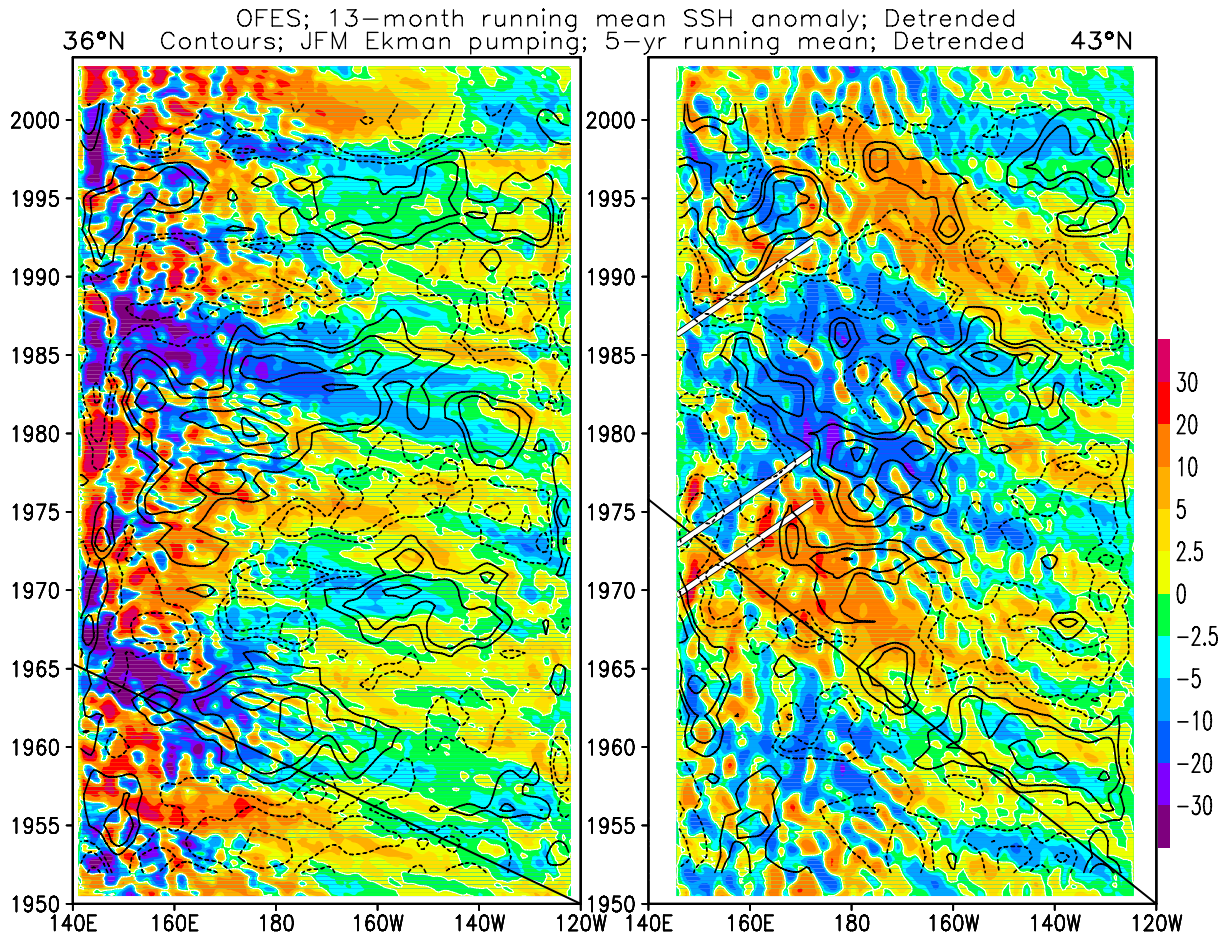

Figure 12. Longitude-time sections of anomalies of SSH (color shading as indicated to the right of the figure; unit: cm) and Ekman pumping (black contours for ±0.25, 0.5, 1.0, 1.5 x10^{-4} cm s^{-1}; dashed for negative values) at (left) 36°N and (right) 43°N. 13-month and five-year running means have applied to the SSH and Ekman pumping anomalies, respectively, and their linear trends have been removed. A thick black line plotted in each of the panels indicates the theoretical propagating speed of the first baroclinic Rossby waves for each of the latitudes. Thick white lines are plotted in the right panel for tracing possible vestiges of eastward-propagating signals.

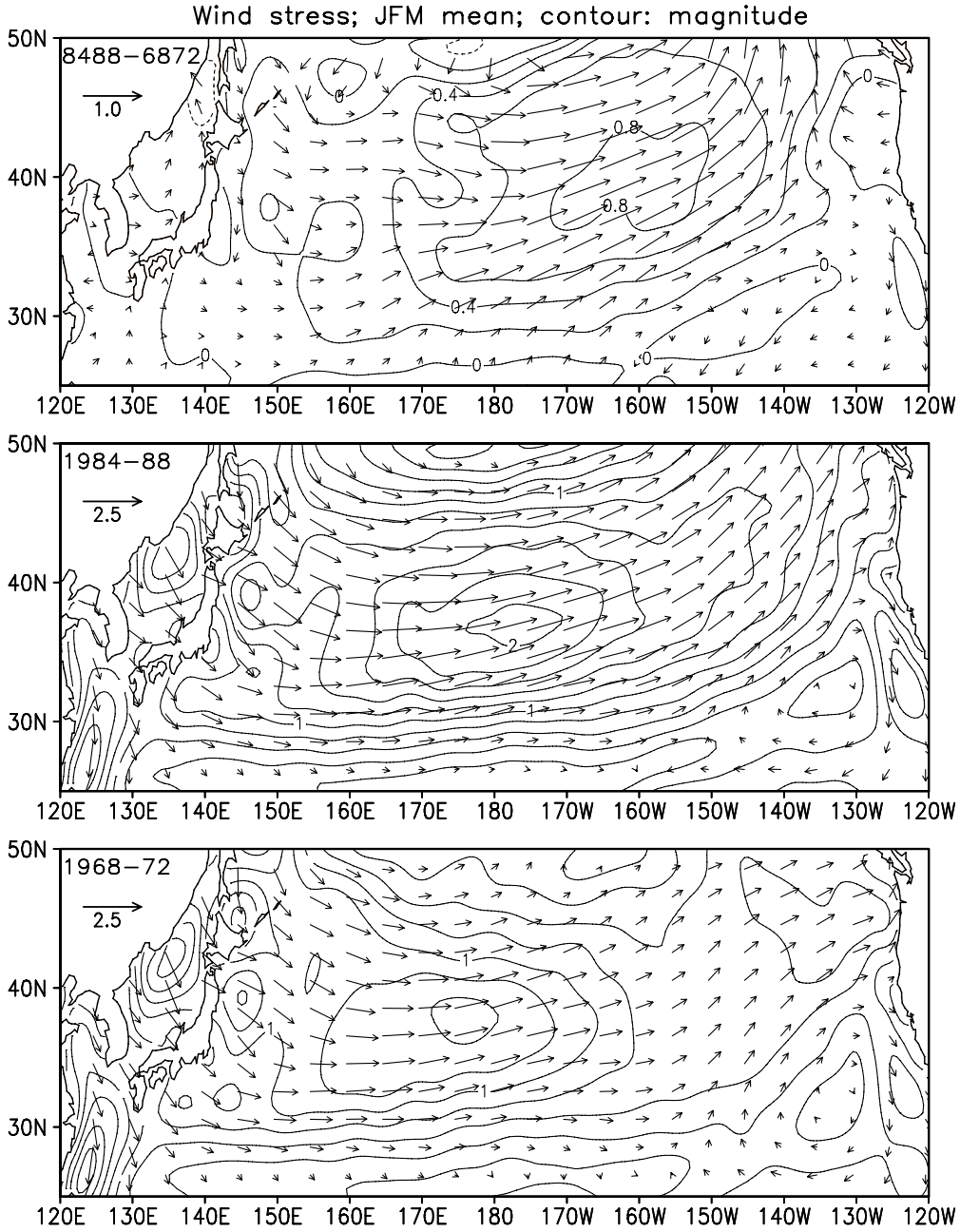

Figure 13. Sea surface wind-stress vectors and its magnitudes (contour intervals: 0.2 dyn cm^{-2}), which forced the OFES simulation, averaged over the five winters (January-March) separately for (middle) 1984-88 and (bottom) 1968-72. The scaling for the vectors (unit: dyn cm^{-2}) is indicated near the upper-left corner of each panel. The difference fields from the earlier period to the later are indicated in the top panel.

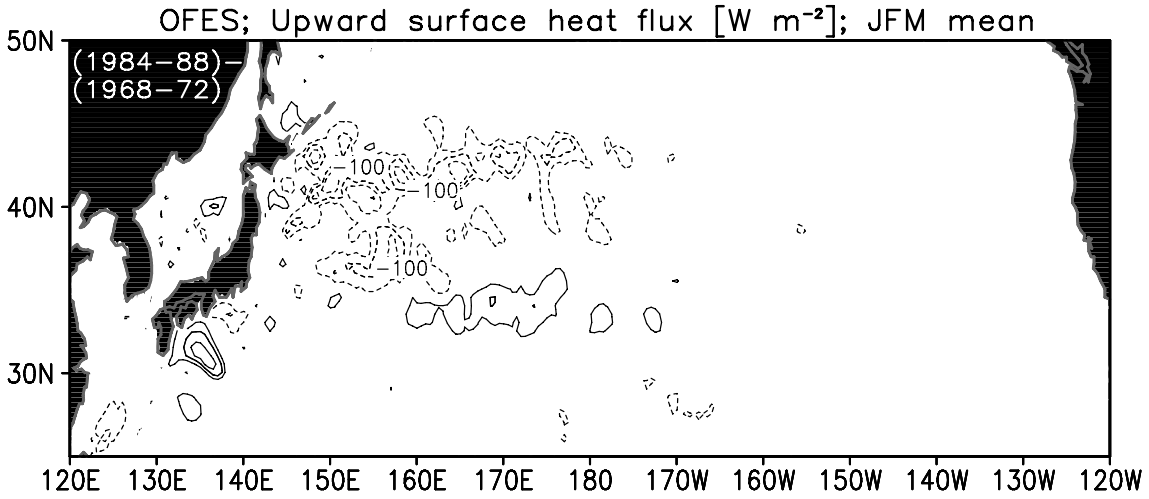

Figure 14. Mean difference map of the net upward heat flux at the surface from five-year period 1968-72 to another five-year period 1984-88. Contour intervals are 50 (W m^{-2}), and negative values are dashed (zero lines are omitted). Based on the OFES simulation for winter (January-March).

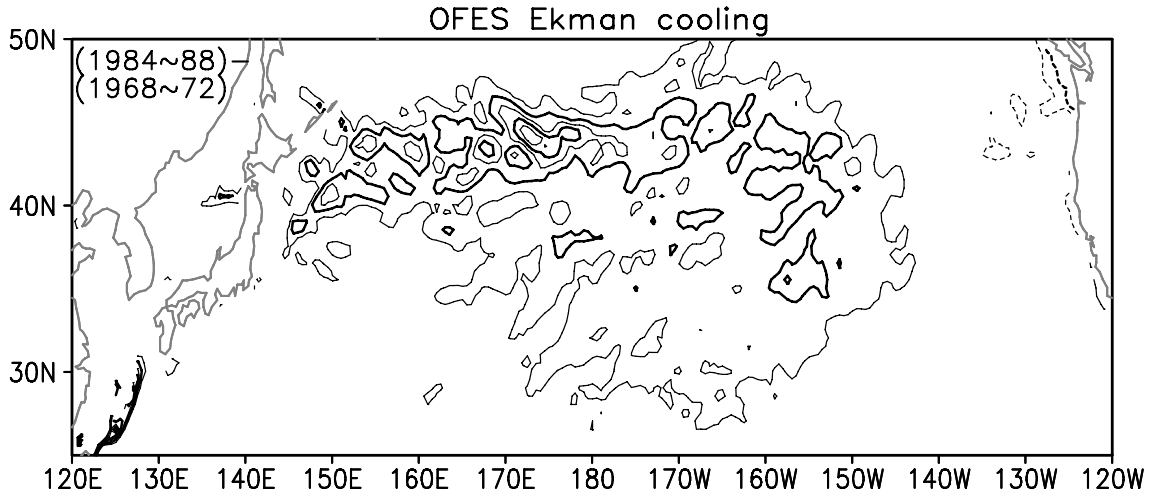

Figure 15. Contribution of changes in the surface Ekman advection induced by the corresponding changes in the wind stress to the SST differences between 1984-88 and 1968-72, based on the OFES simulation. For each of the five-year periods, the contribution has been evaluated locally as the mean January-March SST difference due solely to the five-year mean Ekman transport anomaly acting on the same five-year mean SST both for the whole winter season (October through March), by assuming the mixed layer depth to be fixed to its January-March mean value during the particular five-year period. The difference in the contributions estimated as above is plotted for every 0.25°C with heavy lines for every 0.5°C. Negative (i.e., enhanced cooling) values are solid, and the zero contours are omitted.